Variations in Atterberg Limits for the Lawton Clay with Acidic Pore Fluids

Esten King

A report prepared in partial fulfillment of the requirements of the degree of

Master of Science
Earth and Space Science: Applied Geosciences

University of Washington

March 2020

Reading Committee:
Kathy Troost
Mike Brown

MESSAGe Technical Report Number: [083]

Executive Summary

The physical mechanisms that cause slope failure involving the Lawton Clay in the Puget Lowland have been well studied; however, the physio-chemical mechanisms, specifically acidic pore fluid are poorly understood. This study attempts to quantify the effect of pore fluid acidity on the Lawton Clay's plasticity through Atterberg Limit tests. I conducted multiple runs of the liquid limit and plastic limit tests on rehydrated, homogenized samples of Lawton Clay with acidic solutions mimicking the composition of acid rain in the Seattle area at a pH range of 3.5 to 7. My results show a trend of increasing and then decreasing liquid limit with increasing acidity. This trend is best explained by changes in the thickness of the double diffuse layer and clay minerals' ability to attract water to its surface. The changes in Atterberg Limits can be used as a proxy for changes in strength. The liquid limit results suggest that variations in pore fluid pH could affect the strength of the Lawton Clay and hence be an important variable in slope stability.

Acknowledgements

I would like to thank Mr. John LaManna for helping with the inception of this project and providing insight into the clay mineralogy of the Seattle area. I would also like the thank Dr. Michael Gomez from the University of Washington's Civil and Environmental Engineering department. He provided lots of information on clay mineralogy and clay – water interactions. In addition, Michael offered to train me in the simple shear test before my project changed scope.

My reading committee consisted of Dr. Kathy Troost and Dr. Michael Brown, who both greatly improved the quality of my work. I would like to thank Mike for the critical review of my findings, specifically in how my data and error is presented. I would like to thank Kathy for presenting this project idea to me in the first place and helping me see it through to the end. All of my analysis took place in her lab using her equipment. In addition, she even came down and did a few Atterberg Limit tests with me.

Contents

List of Figures

List of Tables

1.0 Introduction

Landslides are a common natural hazard in the Puget Lowland. Previous investigations have studied the physical mechanisms that cause slope failures in the Puget Lowland (Badger and D'ignazio, 2018; Godt and Mckenna, 2008; Harp et al., 2008). A typical cause of slope failure in the region is an increase in pore pressure adjacent to the contact of the Lawton Clay and overlying advance outwash (Tubbs, 1974). During precipitation events and through the entire wet season (September – May), rainwater infiltrates through advance outwash and pools on top of the Lawton Clay due to its relative impermeability. Water saturates the advance outwash causing an increase in pore pressure, decreasing the overall stability of the slope (Savage et al., 2000).

Another style of failure that produces larger landslides are those that have deep-seated failure planes within or through glaciolacustrine deposits. Notable deep-seated landslides in the Puget Lowland include the Perkins Lane, Woodway, Possession Bay, and Oso landslides. The Woodway, Possession Bay, and Oso landslides failed along novel failure planes through the entire Vashon sequence, including glaciolacustrine deposits. The role of seasonal changes in pore pressure within the glaciolacustrine deposits is unclear and other factors could be responsible for a loss of strength within the unit (Badger and D'ignazio, 2018).

One potential factor causing the loss of strength within the Vashon glaciolacustrine deposits is the physio-chemical effects of acidic rainwater. Acidic rainwater could play an increasingly important role in slope stability in the fast-growing urban area of the Puget Lowland. Urban areas such as the Seattle area have the potential for increased levels of acidity in its rainwater (Parungo et al., 2002). Currently, there is a lack of information on how the acidity of pore fluids affects the strength and plasticity of the Vashon glaciolacustrine deposits, specifically the Lawton Clay. The goal of this study is to determine the relationship, or lack thereof, between pore fluid acidity and plasticity in the Lawton Clay using Atterberg Limit tests. The potential relationships between pore fluid pH and strength could be an important factor to consider in deep-seated landslides.

2.0 Background

2.1 Geologic Setting

The Lawton Clay is an extensive proglacial lacustrine deposit in the Seattle area (Figure 1). The Cordilleran ice sheet reached the Seattle area about 17,400 years ago (Porter and Swanson, 1998). The advancing ice sheet split into two lobes, the Puget Lobe and Juan de Fuca Lobe, as the ice sheet advanced south from British Columbia (Porter and Swanson, 1998). The Juan de Fuca lobe blocked drainage flowing north through the Puget Lowland (Porter and Swanson, 1998). As a result, proglacial lakes formed in low lying topography as the Puget Lobe ice sheet advanced and dammed north flowing streams (Armstrong et al., 1965). The lake level was defined by the Leland Creek spillway (near present day Port Townsend) to the north and the Black Lake spillway (near present day Olympia) to the southwest (Thorson, 1989). It was during this stage of the Puget Lobe advance that the bottom unit of the Vashon Drift, the Lawton Clay, was deposited in freshwater/brackish proglacial lakes (Armstrong et al., 1965; Booth, 1994).

The Lawton Clay consists primarily of laminated clay and silt. Silt appears as thin, light grey layers, while clay layers are thicker and darker grey (Mullineaux, 1967) (Figures 2, 3). Fine sand beds are interbedded with the Lawton Clay at the top and bottom of the unit. Vertical and horizontal fracture sets orientated orthogonally are common to the Lawton Clay and are likely associated with loading and unloading from ice advance/retreat. The Lawton Clay extends through much of northwestern and southwestern Seattle (Figure 1A) between the elevations of 21 to 45 m above mean sea level (meters AMSL) (Troost and Booth, 2008). It also extends through the central business district and northeastern part of Seattle at elevations of 30 to 55 m AMSL (Mullineaux, 1967). The average thickness of the Lawton Clay is approximately 24 m (Troost and Booth, 2008).

Mullineaux (1967) found the clay mineral composition in order of decreasing abundance: chlorite, illite, and montmorillonite (a mineral in the smectite group). Gault (2015) used an X-ray Diffractometer (XRD) to confirm the clay mineral composition of the Lawton Clay at six locations across the Puget Lowland. Gault found that the clay mineralogy of the Lawton Clay is consistent across the Puget Lowland with chlorite, illite, and smectite. In addition, Gault (2015) found that the non-clay minerals present at the 2-micron grain size are

amphibole and plagioclase. The clay minerals present in the Lawton Clay are detrital (Mullineaux, 1967).

In the typical advance glacial sediment package, advance outwash (Esperance Sand) overlies the Lawton Clay (Figure 4). Advance outwash is a proglacial fluvial and lacustrine sand with interbeds of silt/clay (Mullineaux et al., 1965). The beds directly overlying the Lawton Clay at Discovery Park (the type section location for the Lawton Clay) are transitional deltaic-lacustrine bottomset sand and silt/clay (Mullineaux et al., 1965). The Esperance Sand conformably transitions upward to clean sand and gravel deposited in large outwash plains by braided streams. The uppermost unit in the Vashon Drift glacial sediment sequence at Discovery Park is the Vashon basal till. It was deposited on top of the other proglacial Vashon Drift sediments underneath the advancing ice sheet. The Vashon till is gap graded, very dense silty sand and gravel with cobbles and boulders. The till has low permeability but contains occasional sand or gravel lenses and voids or joints that have high hydraulic conductivities increasing the bulk unit permeability. All of the Vashon Drift sediments were consolidated by up to 1000 m of ice in the Seattle area (Thorson, 1989). All of the Vashon Drift units have varying thicknesses and lateral continuity. (Troost et al., 2005).

In much of Seattle the Esperance Sand is exposed at the ground surface and directly overlies the Lawton Clay (Figure 1). The Lawton Clay can support near vertical faces and makes up many steep slopes and bluff faces in the Seattle area (Troost and Booth, 2008). In areas where there is a cap of Vashon till over the Esperance Sand, infiltration of rainwater can still happen quickly because of joints and sand lenses in the Vashon till that have high hydraulic conductivity. Glacial scouring and sporadic deposition by glaciers have resulted in unconformities and stratigraphy differing from that mentioned previously. In parts of the Seattle area Vashon till directly overlies the Lawton Clay or sediments from older glacial advances or interglacial periods (Troost and Booth, 2008).

2.2 Acid Rain

Acid rain is caused by the oxidation of sulfate (SO_2) and (NO_2) with atmospheric hydroxide (OH) to form sulfuric acid (H_2SO_4) and nitric acid (HNO_3), respectively (Parungo et al., 2002). SO_2 and NO_2 are primarily emitted from the burning of fossil fuels. Urban areas with

higher rates of fossil fuel consumption typically have more acid rain compared to rural areas. The atmospheric concentration of hydrogen ions expressed as pH in Washington ranged from 5.3-5.5 in 2017 (NADP, 2017) (Figure 5). The atmospheric H+ ion concentration is analogous to the rainwater pH. Measurements of wet soil pH from the Washington Department of Ecology (2019) range from about 5 – 10 in the Puget Lowland (Figure 6), much more than the atmospheric pH.

I made the assumption that the pH of rainwater is not being significantly buffered during infiltration in locations where the Esperance Sand is exposed at the ground surface. The Esperance Sand has silt lenses, little to no organics, and is generally unoxidized (Troost and Booth, 2008) making the unit relatively chemically non-interactive. Sand has a low CEC (3-5 meq/100 g) and the residual acidity after cation exchange would have low buffering capacity (Weil and Brady, 2016). In addition, infiltration rates are high in sands and gravels (4 – 10 in/hr) in the Seattle area further reducing the time available for chemical interactions (Massman and Butchart, 2001).

2.3 Clay Minerals

Clay minerals, formed by the weathering of other silicate minerals, have repeating sequences of silica tetrahedral and alumina octahedral sheets. How these sheets stack impacts the swelling capacity and reactivity of the clay mineral (Mitchell, 1993). The clay minerals present in the Lawton Clay are all 2:1 structure, meaning that an octahedral (O) sheet is confined between two tetrahedral (T) sheets in a T-O-T layer (Appendix, Figure A-1). Each of the 2:1 clay minerals differ in how the T-O-T layers are bonded. The ability of the clay surface to substitute cations on its surface, called the cation exchange capacity (CEC), varies with clay mineralogy.

Considering the clay minerals present in the Lawton Clay, illite contains potassium ions that strongly bond layers making it non-expansive (Mitchell, 1993). Illites have a CEC of 10 to 40 meq/100 g (equivalent to centimoles of charge per kilogram of soil). Unlike other clay minerals, chlorite's T-O-T layers are bonded by a positively charged octahedral sheet with a chemical formula similar to the mineral brucite (Mitchell, 1993). Chlorite is considered non-expansive due to this strong bond. Chlorites have a CEC of 10 to 40 meq/100 g similar to illite. In contrast, smectite has layers bonded by cations and van der Waal forces to balance structural

charge deficiencies in the T-O-T sheets. These bonds are weak and can expand with the absorption of water or other polar liquids (Mitchell, 1993). Smectite minerals have a high CEC of 80 to 150 meq/100 g.

Sequences of repeating T-O-T layers build clay particles into the shape of a platelet. Clay platelets have a large specific surface due to the face of the platelet having a much larger area than the edges. Clay platelets are then attracted to each other via electrostatic forces to form structures of multiple clay platelets creating flocs in a process called flocculation. Clay platelets can floc together in face to face or edge to face structures. The amount of flocculation and the orientation of clay platelets within flocs are a major contributor to a clay soil's cohesion. The greatest cohesion occurs in a highly flocculated soil with edge to face flocs (Mitchell, 1993).

The strength of soils with clay minerals is impacted by pore fluids. Clay platelets adsorb water to their surface through electrostatic forces, hydrogen bonding, and cation bonding. The layer of water that is attracted to the clay particle's surface is called the adsorbed water layer (Mitchell, 1993). Clay platelets have a permanent negative charge that forms from isomorphous substitution. The permanent negative charge is balanced by temporary cation substitutions on the edge of clay platelets (Mitchell, 1993). The Gouy-Chapman-Stern model (Appendix Figure A-5) gives a simplified schematic of how cations are temporarily attracted and adsorbed to the clay surface. Cations are attracted to the negative charge of the clay platelet surface. A layer of cations are adsorbed directly onto the clay platelet surface (Van Olphen, 1963). The space occupied by the first layer of cations on the surface depends on the ionic radius and charge of the cation. After the first layer, cations in the pore fluid are attracted to the surface through the Coulomb force and are free to travel through the pore fluid surrounding the clay platelet. These loosely held cations make up a diffuse potential of positive charge. The cation concentration (and positive potential) decreases with distance from the clay surface as the affinity to the negatively charge clay surface decreases. Eventually at some distance the cation concentration equals the bulk solution concentration. The thickness of the adsorbed cations and increased cation concentration (diffuse layer) in solution is the double diffuse layer. In general, thinner double layer thickness results in flocculation while thicker double layer thickness results in dispersion of clay particles (Mitchell, 1993).

2.4 Atterberg Limits

The Atterberg Limit test distinguishes the boundaries of consistency states in plastic fine-grained soils by measuring the water content at these states (ASTM D4318-10). In fine-grained soils, strength is closely related to how the soil deforms under stress, which is ultimately a function of water content (Mitchell, 1993). The liquid limit is the boundary between semi-liquid and plastic consistency states. The undrained shear strength at the liquid limit is approximately 2 kPa (ASTM D4318-10). The plastic limit is the boundary between plastic and semi-solid consistency states. A plastic soil will retain its shape when drying. The plasticity index is the range of water contents under which a fine-grained soil behaves plastically (ASTM D4318-10). Atterberg Limits have empirical correlations to compressibility, permeability and strength (Holtz et al., 2011). The Atterberg Limit test has repeatability error due to differences between operators and procedural variation for single operators (ASTM D4318-10).

At a fundamental level the liquid limit measures the volume of water adsorbed to the surface of clay particles. Thickening or thinning of the adsorbed water layer will result in increases or decreases to the volume of adsorbed water. The liquid limit should be sensitive to changes in the adsorbed water layer thickness. Another factor that changes the volume of adsorbed water is the mineralogy. The average thickness of that adsorbed water layer is consistent between clay minerals with similar pore fluid conditions. The liquid limit is different for different clay minerals because the volume of water is dependent on the specific surface of the clay mineral (Mitchell, 1993). The volume of adsorbed water increases as the specific surface increases. For this study a homogeneous mineralogy will constrain variations in liquid limit to changes in adsorbed water layer thickness.

2.5 Previous Research

Although the effect of acidic pore fluid on the strength of the Lawton Clay has not been investigated, other studies have focused on fine-grained soils. In a series of studies (Gratchev and Sassa, 2013; Gratchev and Towhata, 2009; Gratchev and Towhata, 2011; Gratchev and Towhata, 2016; Gratchev and Towhata, 2013) the effects of long-term acidic pore fluid contamination on fine-grained soils in Japan were examined. Naturally occurring fine-grained soils were saturated at various timescales (up to 300 days) to simulate acidic contamination. They measured

engineering properties of the contaminated soils (consolidation, Atterberg Limits, triaxial undrained compression test, direct shear test, and compressibility). They found that samples exhibited complex trends in the engineering properties. The clay minerals present, relative percentages of clay minerals, and soil structure were important factors to how the bulk soil responded to increased acidity. For example, Gratchev and Towhata (2009) found that the Osoka Bay clay and Ariake clay had increased compressibility when subjected to long term acidic contamination, while the Kawasaki mud had decreased compressibility in the same conditions. The Osoka Bay clay is comprised of smectite, chlorite, kaolinite, and illite with relatively high amounts of carbonates including microfossils. The Ariake clay has a composition of smectite, kaolinite, illite, and vermiculite. The Kawasaki mud is mainly montmorillonite and chlorite.

3.0 Methods

3.1 Sample Collection

Gault (2015) found that the mineralogy of the Lawton Clay is consistent throughout the Puget Lowland. As such, I decided that samples collected from one location would be representative of the bulk unit properties found in the Puget Lowland. I collected block samples from Discovery Park, Washington, the type section for the Lawton Clay (Figure 7). I focused sampling to the middle of the stratigraphic section to avoid transitional sand interbeds at the top and bottom of the section. At this location there are exposed bluff faces (Figure 8) of Lawton Clay and fallen blocks from higher up in the section. The bluff face is too steep to sample a vertical profile without use of climbing equipment. I only collected blocks without sandy interbeds.

3.2 Sample Processing

After collecting samples of Lawton Clay from the bluff face at Discovery Park, I measured the in-situ water content following ASTM D-2216. My samples had an in-situ water content of 27.7% and a liquidity index (LI) of 0.38. A liquidity index of 0.38 indicates that

material at the in-situ water content is below the liquid limit and above the plastic limit and will deform as a plastic.

I prepared samples with the intention of isolating the interaction between pore fluid acidity and strength. The Lawton Clay is varved and therefore has natural variations in clay and silt content at the millimeter scale (Figures 2, 3). The Woodway, Possession Bay, and Oso landslides failed along failure planes that cut through the varves in the Lawton Clay. In these cases, I assumed that the strength of the bulk unit is important. To get a close approximation of bulk unit characteristics, I homogenized block samples of varved Lawton Clay to evenly distribute the clay and silt content. Inconsistencies in silt and clay content could obscure the interaction between pore fluid acidity and strength. I air dried the blocks of Lawton Clay to remove the in-situ pore fluid. The drying process also allowed for easier sample homogenization and later re-hydration with acidic solutions. Prior to starting the homogenization process, I scraped off sand that contaminated the blocks during collection. The first step of homogenization was to break the blocks into smaller pieces (10 cm or less). The broken pieces of Lawton Clay dried for four weeks on a plastic tarp in an enclosed but ventilated area allowing for air circulation without risk of contamination by rain (Figure 9). The broken pieces were hand mixed every week to ensure even drying. After the 4-week drying process, I broke up the remaining larger pieces into <2.5 cm pieces. The homogenized samples of Lawton Clay continued to dry in large sample bags until the rehydration process began.

I sent in six samples to the Soil Analytics Lab and Analytical Service Center at the University of Washington to measure the cation exchange capacity (CEC) of the homogenized soil (Table 1). The average CEC of the six samples is 12.07 meq/100 g.

3.3 Acidic Solutions

I made acidic solutions for this study ranging in pH from 3.5 to 7 at 0.5 intervals to encompass the natural range of pH and conditions that are common in geotechnical practices. The acidic solutions contain the molar proportions of acid rain causing anions (in their acid form) measured in Seattle rainwater by Root et al. (2004). The anions are chloride, nitrate, and sulfate which bond with water to create hydrochloric, nitric, and sulfuric acid respectively. The molarities of the sulfuric and nitric acids were unknown, so I used titration to determine their

molarity. I used a 10 M NaOH titrant made from solid NaOH pellets and de-ionized (DI) water to perform the titration. The acidic solutions are made up of diluted 1M hydrochloric, 16.36M nitric, and 16.07M sulfuric acids. The rainwater anion concentrations, molarities, and molar proportions are shown in Table 2.

After determining the molarities of the concentrated acids, I made three bulk solutions that contained the same molar proportions of the acid molarities mentioned above, but at different H+ concentrations. This retains the molar proportions of the three acidic species, while changing the pH/acidity. I made three bulk solutions with pH values of 3.88, 0.87, and 0.33. The bulk solution with a pH of 3.88 contains the acid molarities mentioned in Table 2. I went through multiple dilutions of the concentrated acids to reduce the molarity. I calculated the volume of DI water needed to dilute a starting volume of acid using the equation $M_1V_1 = M_2V_2$. I checked the pH of the solution with a calibrated Milwaukee 102 pH meter (resolution of 0.01 pH) after each dilution step. This allowed me to check the solution H+ concentration with my theoretical H+ concentration. I used graduated cylinders to measure volume because they were what was available to me at the time of analysis and due to budget constraints. The volumes of acid that I needed to dilute were often small, so the accuracy and precision of the volumes measured by the graduated cylinders was low. Since the molarity is in terms of H+, the molarity can be easily converted to pH. So, I knew both the final molarity and pH for each step in the dilution process. I used the pH meter's measurements as my new starting molarity (after converting it) instead of the calculated molarity because the pH meter's accuracy is greater than that of the graduated cylinder. I used the measured H+ concentration as the initial molarity when calculating volumes for the subsequent dilution step. The 0.87 and 0.33 pH solutions were made using the same procedure, with fewer dilution steps.

3.4 Rehydrating Dry Soil at Various pH Values

Clay minerals buffer the solution pH through cation exchange (Mitchell, 1993). To roughly quantify the buffering capacity of the Lawton Clay in order to predict the initial pH of the acidic solutions to achieve pH values ranging from 3.5 to 7 at 0.5 intervals. I made sulfuric acid solutions at pH = 0.0, 0.92, 1.91, and 2.52 (Figure 10) and nitric acid solutions at pH = 3.0, 4.04, and 4.91. I mixed a ratio of 40/60 soil to solution and measured the pH immediately after

mixing. The viscosity of the mixed sample was low enough to directly measure using the pH meter. I also took pH measurements at 4 days for the sulfuric acid mixtures and 3 days for the nitric acid mixtures. These measurements showed that the buffering capacity is largest when the starting solution pH is between 0.5 and 3. The lower pH solutions also took longer to buffer and reach an equilibrium pH. The complex trend in buffering capacity makes predicting the final soil pH using the initial acidic solution pH difficult. I decided the best course of action was to use the buffering capacity data as a rough guide for initial acidic solution pH.

Using the buffering capacity results as a guide, I diluted the stock solutions from a pH of 0.33 to 6.5, the pH of the de-ionized (DI) water. I then mixed the solutions with dry soil to make eight samples (one for each 0.5 interval at a pH range of 3.5 – 7). After mixing, samples had to be at a low enough viscosity to ensure that I could measure the pH directly with the pH meter. I recorded the pH of each mixture after combination and then at 14 days after the addition of the acidic solutions. Gratchev and Towhata (2016) found that it took about 7 days for the pH of the pore fluid to stabilize. After the samples rested for 14 days and reached an equilibrium pH, I made fine adjustments to the pH. I increased the pH by adding more soil, DI water and/or 0.1M NaOH solution and decreased the pH by adding acidic solution. I confirmed the final pH with the pH meter three days later to allow the soil mixture to reach equilibrium.

I initially underestimated the amount of sample required for Atterberg Limits testing. To increase the amount of sample I went through a similar process as the initial sample rehydration. In this case I added dry soil and DI water to the already prepared samples and then measured the pH directly after mixing and again six days after mixing. I made fine adjustments to the pH after the samples sat for six days using the same method as previously stated. The final pH values of the eight samples were within 0.13 of the goal pH values. I began Atterberg Limits tests eleven days after making the final fine adjustments to the pH.

3.5 Atterberg Limits

I determined the plasticity of the eight rehydrated homogenized samples (pH = 3.49, 4.01, 4.52, 4.87, 5.54, 5.98, 6.48, 6.90) using the Atterberg Limits test procedure described by the American Standards of Testing and Materials (ASTM) in ASTM D4318-10: Standard Test Methods for Liquid Limit, Plastic Limit, and Plasticity Index of Soil (ASTM, 2010). I made the

following exceptions for the Liquid Limit: 1) when remixing the entire soil specimen high moisture content sample or acidic solution was used to increase the water content of the soil in place of distilled water, and 2) multiple runs of the 3-point method liquid limit test (6-11 runs) were conducted at each pH level to increase reproducibility. The ASTM standard procedure for the liquid limit test is to progressively wet the remolded soil sample with distilled water to produce blow counts in the range of 25 to 35, 20 to 30, and finally 15 to 25 (Figure 11). To reduce the risk of changing the pH, I used a high moisture content sample or acidic solution to increase the moisture content of a low moisture content sample. If the initial moisture content was too high (blow count under 15) I remolded the sample on frosted glass to decrease the water content instead of adding dry soil to reduce the risk of altering the pH (Figure 12). If the initial moisture content was too low, as was often the case with samples that had undergone the liquid limit test eight or more times, samples (pH = 4.5, 6.5, 7) were rehydrated with acidic solutions at those pHs. The ASTM standard procedure for the 3-point liquid limit test is to record the water content of the soil sample at a range of 25 to 35, 20 to 30, and finally 15 to 25 blow counts. The liquid limit is the water content at 25 blow counts determined by a best fit line. I did multiple runs of the 3-point liquid limit test at each pH level to increase the accuracy of the liquid limit value. I conducted more runs for pH levels that had large variation around the liquid limit prediction line. The plastic limit tests (Figure 13) were conducted following ASTM D4318-10. I did 4 – 6 runs of the plastic limit test per pH value.

After conducting the Atterberg Limit tests I measured the pH of the remaining soil which was at a lower water content than I originally measured as a result of progressive drying from testing. I could not measure the pH directly from the remaining sample as I did for the original mixed sample, so I mixed even parts distilled water to soil to get the soil to a consistency that the pH meter could read. The pHs of the samples were an average of +/- 0.07 from the starting pH (Table 2).

3.6 Data Processing

I determined the liquid limit by fitting a single linear regression to all the points in water content vs. log (blow counts) at each pH value. The linear regression equation can be solved for

the water content at 25 blow counts, which is how the liquid limit is defined. The error is quantified by a 95% confidence interval.

4.0 Results

I conducted multiple runs of the 3-point liquid limit test at each of the eight pH values (3.49, 4.01, 4.52, 4.87, 5.54, 5.98, 6.48, and 6.90) (Table 4 and 5) (Figures 14-21). The data show that the liquid limit is greatest at a pH of 4.5 with a water content of 36.5% and that the liquid limit decreases on either side of the peak (Figure 22). The minimum liquid limit occurs at a pH of 6.5 with a water content of 34.5%. I also conducted multiple plastic limit tests at the same pH values as the liquid limit tests (Table 6). No significant trend is apparent for plastic limit vs. pH (Figure 23). There is a discernible drop in plastic limit at a pH of 7, but the plastic limits at the rest of the pH values are similar. Similar to the liquid limit, the plasticity index shows a peak at a pH range of 4 - 5 (Figure 24) (Table 7). Unlike the liquid limit values, the plasticity index at near-neutral pH have more variability.

On an Atterberg Limit mineralogy and plasticity chart the samples plot within the illite clay mineral group and above the A-line as a low plasticity clay (CL) (Figure 25). The spread of liquid limits across the eight pH values is small compared to the variation in liquid limits in natural non-homogenized samples. The Lawton Clay can classify as a low plasticity silt (ML), high plasticity silt (MH), low plasticity clay (CL), or high plasticity clay (CH) because of the intrinsic variability within the deposit (Badger and D'ignazio, 2018). While the clay minerals present in the Lawton Clay are consistent the ratio of clay to silt can vary widely between locations and vertically within the unit.

5.0 Discussion

Previous research offers four possible mechanisms that can affect strength as a function of pH. The most likely mechanism responsible for the trend shown in this study is changes in the thickness of the double diffuse layer. The thickness of the double diffuse layer ($\frac{1}{K}$) is governed by the equation:

$$\frac{1}{K} = \sqrt{\left(\frac{\epsilon_0 DkT}{2n_0 e^2 \nu^2}\right)}$$ (Mitchell, 1993).

ϵ_0 = permittivity of a vacuum
D = dielectric constant of the medium
k = Boltzmann constant
T = Temperature (K°)
n_0 = electrolyte concentration
ν^2 = cation valence

Pore fluid pH affects the valence of the cations (ν) and concentration of electrolyte solution (n_0) variables. As acidity increases, pH drops from a neutral pH of 7 and the concentration of H+ ions in solution increases. The H+ ions displace commonly found cations on the clay platelet surface because of H+ ions strong aptitude for adsorption (first place on the Hofmeister Series) even at low concentrations (Gajo and Maines, 2007). The commonly found exchangeable cations in the Lawton clay are Ca^{2+} and Mg^{2+} (Mullineaux, 1967). By replacing cations of greater charge, the valence variable in the double diffuse layer thickness equation decreases, resulting in an increase of the double diffuse layer thickness. As pH decreases past slightly acidic conditions, the increase in concentration of H+ (n_0) overcomes the decrease in valence from displacing higher valence cations (Van Olphen, 1963). This causes a decrease in the thickness of the double diffuse layer. At very acidic conditions the double diffuse layer would collapse entirely (Van Olphen, 1963). This trend of thickening and then thinning double diffuse layer thickness with increasing acidity results in a decrease and then increase in strength because of the tendency of clay particles to disperse with thicker double layers and flocculate with thinner double layers. Flocculation is a key contributor to a soil's cohesion and hence, strength (Mitchell, 1993). The liquid limit values follow the same trend of increasing and then decreasing with increasing acidity. This trend reflects the increase and subsequent decrease in adsorbed water layer thickness. As the double diffuse layer thickness decreases smectite's structure becomes more compact and reduces the amount of pore fluid needed to initiate particle mobilization (Spagnoli et al., 2012). I would expect the strength to be lowest at pH values of 4.0 – 5.0 where the liquid limit values and double diffuse layer thickness are the greatest.

Changes in the double diffuse layer thickness best describe the trend in liquid limit vs. pH as shown in Figure 22. However, other mechanisms can change with pH that vary with mineralogy and have competing effects. For example, dissolution with increasing acidity of

cementation agents including carbonate, organic matter, or iron oxide can increase the liquid limit. This can change soil fabric structure and reduce aggregates (Gratchev and Towata, 2009). Since Lawton Clay was deposited in predominantly freshwater conditions, dissolution of carbonate cementation is less likely to play a role than in marine deposited clays (Mullineaux et al., 1965). Mullineaux et al. (1965) describe the occurrence of occasional flat calcareous concretions within thin silt layers. It is possible that dissolution of these concretions could impact the liquid limit if present. I did not observe any concretions in my samples. Furthermore, organic matter is not common in the Lawton Clay and none was observed in the current material. In addition, the samples were powdered and remolded during sample preparations reducing the likelihood of depositional conditions influencing the results.

Another mechanism that can change the liquid limit with increasing acidity is preference of edge to face flocculation structures. As previously mentioned, the edges of clay platelets become increasingly positively charged as H+ ions are adsorbed to the platelet surface as H+ concentration increases (Mitchell, 1993). This creates an open flocculation structure that results in higher liquid limits (Mitchell, 1993). This effect is most pronounced in soils with kaolinitic mineralogy. Previous mineralogy studies of the Lawton Clay show that the clay minerals present are illite, chlorite, and smectite (Mullineaux, 1967) (Gault, 2015). Since kaolinite is not a major mineral constituent in the Lawton Clay, the effect of open flocculated structures is not likely a major factor in the changes in liquid limit observed.

It is also possible that differences in pore fluid density could cause mechanical changes during the liquid limit test. The density of the pore fluid increases with decreasing pH as sulfuric, nitric, and hydrochloric acid make up a greater proportion of the pore fluid. This was apparent in the samples mixed with sulfuric acid while constraining the buffer capacity (Figure 10). At lower concentrations of sulfuric acid the soil was more compressed.

There are empirical correlations that show that lower plasticity indexes result in greater internal friction angles (Holtz and Kovac, 2011). Using the Mohr-Coulomb shear strength equation (Appendix Equation 3), greater friction angles increase the shear strength. The plasticity indexes of my samples peak at pH 4.0 – 5.0. These pH values would correlate to a decrease in strength. These pH values are coincident with the loss in strength caused by changes in the thickening of the double diffuse layer and adsorbed water layer that is shown in the liquid limits.

6.0 Limitations

The Atterberg Limit tests have many possible user-derived sources of error. Possible sources of user error for the liquid limit include: blow count rate, soil pat volume, groove straightness, and adequate sample mixing. I tried to maintain consistency in these variables, however any slight deviation in one or more of these variables between runs can affect the results. In this study I aimed to quantify the relative changes in plasticity with differing pore fluid pH. This required me to have repeatability between runs. My repeatability error can be seen in the spread of the 3-point tests results (Figures 14-21) and the prediction error and standard deviations in the liquid limit. Kathy Troost did multiple runs (2-4) of the 3-point liquid limit test at pHs of 4.01, 4.52, and 4.87. She got liquid limit results consistently lower than mine by about 5%. This illustrates the variability of the liquid limit and plastic limit tests between operators. My error ranged between 1% – 5% for liquid limits and 1% – 7% for plastic limits. I did not include Dr. Troost's results in my analysis to reduce reproducibility error between operators.

7.0 Conclusion

This study shows that the plasticity of homogenized samples of Lawton Clay is affected by pore fluid acidity. The liquid limit and plasticity index have coincident peak values when the pore fluid is slightly acidic (pH 4.0 – 5.0). The changes in liquid limit are best explained by a trend of increasing and then decreasing double diffuse layer and adsorbed water layer thickness with increasing acidity. I would expect the lowest strength values to occur at the peak values for liquid limit and plasticity index at a pH of 4.0 – 5.0. Currently the pH of rainwater in the Seattle area ranges from 5.3 – 5.5. My data suggests that a decrease in rainwater pH to 4.0 – 5.0 could result in a decrease in strength in the Lawton Clay. These changes in strength could be important factors to consider for slope stability problems where the Lawton Clay is involved. However, my results do not give any quantitative information on the magnitude of strength changes associated with the increased liquid limit and plasticity index values with slightly acidic pore fluids.

Further study is required to fully quantify the strength of the Lawton Clay in response to acidic pore fluid. I suggest direct or simple shear tests, to measure shear strength values like peak shear strength, residual shear strength, and friction angle. In addition to more comprehensive

strength testing, I suggest research aimed at better constraining the pH of pore fluid present at the contact between the Esperance Sand and Lawton Clay. For this study I assumed that the pH of rainwater will be unaffected by infiltration through the Esperance Sand. Data on pH at depth could be accomplished by pH data loggers installed progressively down a borehole through the Esperance Sand into the Lawton Clay. Another method could be to measure the pH of springs seeping from the contact between the Esperance Sand and Lawton Clay before and after precipitation events. In addition, I suggest an evaluation of future acid rain conditions in the Seattle area with the rapidly growing population. An increase in the acidity of rainwater from the current conditions (pH = 5.2 – 5.5) could decrease the strength of the Lawton Clay.

8.0 References

Abbas, H.O., 2018, Assessment of accuracy in determining Atterberg limits for four Iraqi local soil laboratories: *IOP Conference Series: Materials Science and Engineering*, Vol. 433, No. 1, 9 p.

Armstrong, J.E., Crandell, D.R., Easterbrook, D.J., Noble, J.B., 1965, Late Pleistocene stratigraphy and chronology in southwestern British Columbia and northwestern Washington: *Geological Society of America Bulletin*, Vol. 76, pp. 321-330

ASTM, 2010, Standard D4318 – 10e1, Standard Test Methods for Liquid Limit, Plastic Limit, and Plasticity Index of Soils: West Conshohocken, Pennsylvania, ASTM International.

Badger, T.C., and D'Ignazio, M., 2018, First-time landslides in Vashon advance glaciolacustrine deposits, Puget Lowland, U.S.A.: *Engineering Geology*, Vol. 243, pp. 294–307.

Booth, D.B., 1994, Glaciofluvial infilling and scour of the Puget Lowland, Washington, during ice-sheet glaciation: *Geology*, Vol. 22, pp. 695-698

Gajo, A., and Maines, M., 2007, Mechanical effects of aqueous solutions of inorganic acids and bases on a natural active clay: *Geotechnique*, Vol. 57, No. 8, pp. 687–699.

Gault, A., 2015, *The mineralogy and strength characteristics of selected glaciolacustrine clays in the Puget Sound region*: Unpublished M.S. Thesis, Department of Earth and Space Sciences, University of Washington, Seattle, WA, 60 p.

Gratchev, I.B., and Towhata, I., 2011, Compressibility of soils subjected to long-term acidic contamination: *Envrionmental Earth Sciences*, Vol. 64, No. 1, pp. 193-200.

Gratchev, I.B., and Sassa, K., 2013, Cyclic shear strength of soil with different pore fluids: *Journal Geotechnical Geoenvironmental Engineering*, Vol. 139, No. 10, pp. 1817–1821.

Gratchev, I.B., and Towhata, I., 2009, Effects of acidic contamination on the geotechnical properties of marine soils in Japan. *In Proceedings of the International Offshore and Polar Engineering Conference*, International Society of Offshore and Polar Engineers, Osaka, Japan, pp. 151–155.

Gratchev, I., and Towhata, I., 2016, Compressibility of soils containing kaolinite in acidic environments: *KSCE Journal Civil Engineering*, Vol. 20, No. 2, pp. 623–630.

Gratchev, I., and Towhata, I., 2013, Stress-strain characteristics of two natural soils subjected to long-term acidic contamination: *Soils Foundations*, Vol. 53, No. 3, pp. 469–476.

Godt, J.W., and Mckenna, J.P., 2008, Numerical modeling of rainfall thresholds for shallow landsliding in the Seattle, Washington, area: *GSA Reviews in Engineering Geology*, Vol. 20, pp. 121-136.

Harp, E.L., Michael, J.A., Laprade, W.T., 2008, Shallow landslide hazard map of Seattle, Washington: *GSA Reviews in Engineering Geology*, Vol. 20, pp. 67-82.

Holtz, R., and Kovacs, W., 2011, *Introduction to Geotechnical Engineering,* No. Ed. 2. Pearson, Upper Saddle River, NJ, 853 p.

Laprade, W.T., and Tubbs, D.W., 2008, Landslide mapping in Seattle, Washington: *GSA Reviews in Engineering Geology*, Vol. 20, pp. 37-54.

Massman, J. W., and Butchart, C.D., 2001, *Infiltration Characteristics, performance and design of storm water facilities*: Washington State Transportation Commission, 32 p.

Mitchell, J., 1993, *Fundamentals of Soil Behavior*: No. Ed. 2. John Wiley and Sons, Inc., New York, NY, 599 p.

Mullineax, D.R., 1967, *Gross composition of Pleistocene clays in Seattle, Washington*: Geological Survey Professional Paper 575-B, pp. 69-76.

Mullineaux, D.R., Waldron, H.H., and Rubin, M., 1965, *Stratigraphy and chronology of late interglacial and early Vashon glacial time in the Seattle area, Washington*: Geological Survey Bulletin 1194–0, pp. 1–10.

Parungo, F., Nagamoto, C., and Maddl, R., 2002, A study of the mechanisms of acid rain formation: *Journal Atmospheric Sciences*, Vol. 44, No. 21, pp. 3162–3174.

Porter, S.C., and Swanson, T.W., 1998, Radiocarbon age constraints on rates of advance and retreat of the Puget Lobe of the Cordilleran Ice Sheet during the last glaciation: *Quaternary Research*, Vol. 50, No. 3, pp. 205–213.

Root, E., Jones, W., Schwarz, B., Gibbons, J., Haileab, B., and November, A., 2004, *Rainwater Chemistry Across the United States*: Unpublished, University of North Carolina, Wilmington, NC, 23 p.

Savage, N.Z., Morissey, M.M., and Baum, R.L., 2000, Geotechnical Properties for Landslide-Prone Seattle Area Glacial Deposits: US Geological Survey Open File Report 00-228, pp. 1 – 5.

Spagnoli, G., Rubinos, D., Stanjek, H., Fernández-Steeger, T., Feinendegen, M., and Azzam, R., 2012, Undrained shear strength of clays as modified by pH variations: *Bulletin of Engineering Geology and the Environment*, Vol. 71, pp. 135–148.

Thorson, R.M., 1989, Glacio-isostatic response of the Puget Sound area, Washington: *Geological Society America Bulletin*, Vol. 101, No. 9, pp. 1163–1174.

Troost, K.G., and Booth, D.B., 2008, Geology of Seattle and the Seattle area, Washington: *GSA Reviews in Engineering Geology*, Vol. 20, pp. 1–35.

Tubbs, D.W., 1974, Landslides in Seattle: Washington State Department of Natural Resources, Division of Geology and Earth Resources, Circular No. 52.

Van Olphen, H., 1963, *Clay Colliod Chemistry*: John Wiley & Sons, New York, NY, 301 p.

Weil, R. R., Brady, N. C., 2017, *The Nature and Properties of Soils:* Pearson Press, Upper Saddle River, NJ, 1086 p.

Figures

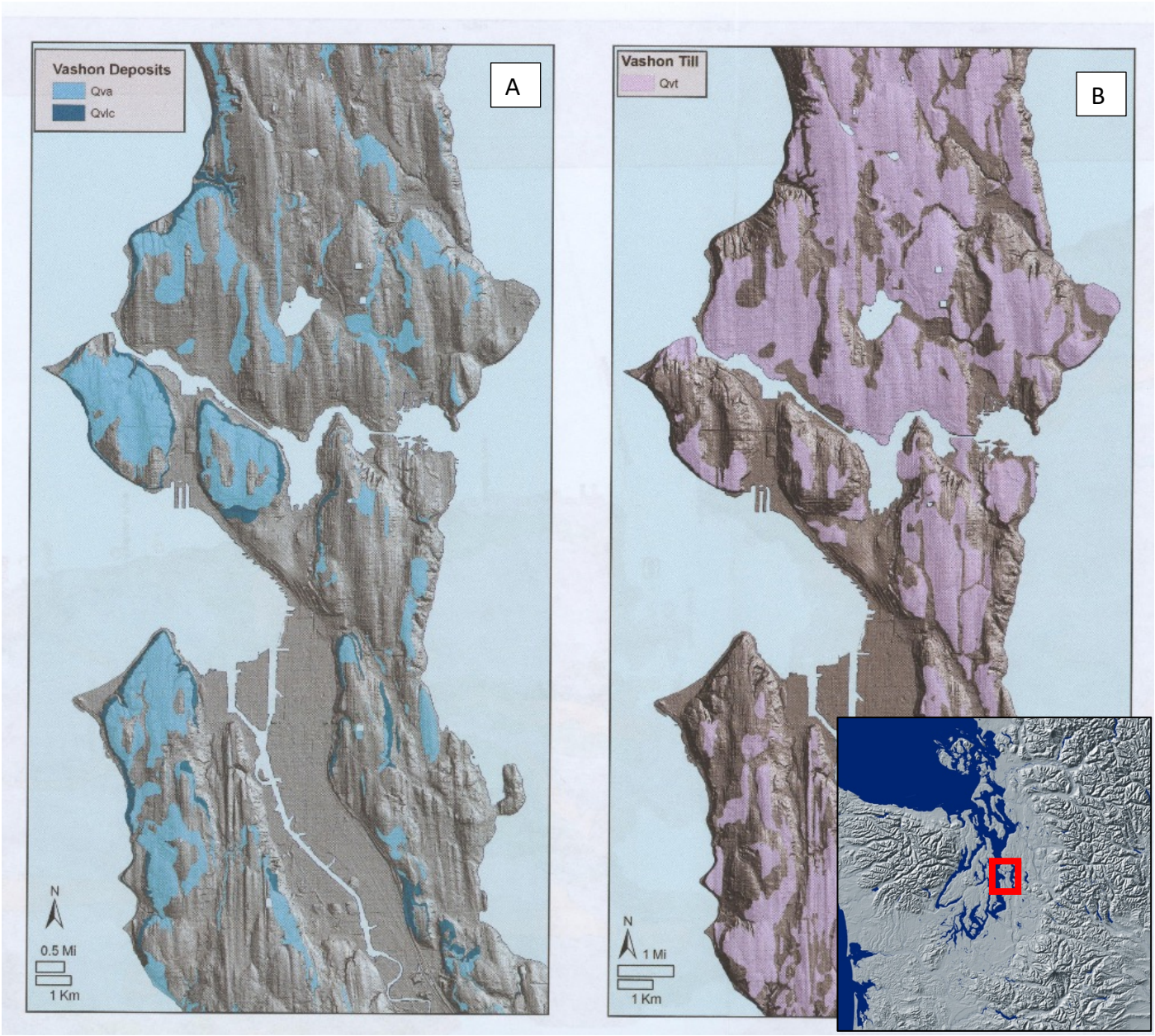

Figure 1. A (left) – Outcrops of Lawton clay in the Seattle area (dark blue) overlain by the Esperance Sand (light blue) without Vashon till cap. **B** (right) – Extent of Vashon till at ground surface in the Seattle area. (Adapted from Troost and Booth, 2008)

Figure 2. Block sample of Lawton Clay consisting of laminated clay and silt. Silt appears as thin, light grey layers, while clay layers are thicker and darker grey. There are local ripple marks. Scale is in centimeters.

Figure 3. Close up view of the sedimentary structures in the Lawton Clay. Silt appears as thin, light grey layers, while clay layers are thicker and darker grey. There are local ripple marks. Scale is in centimeters.

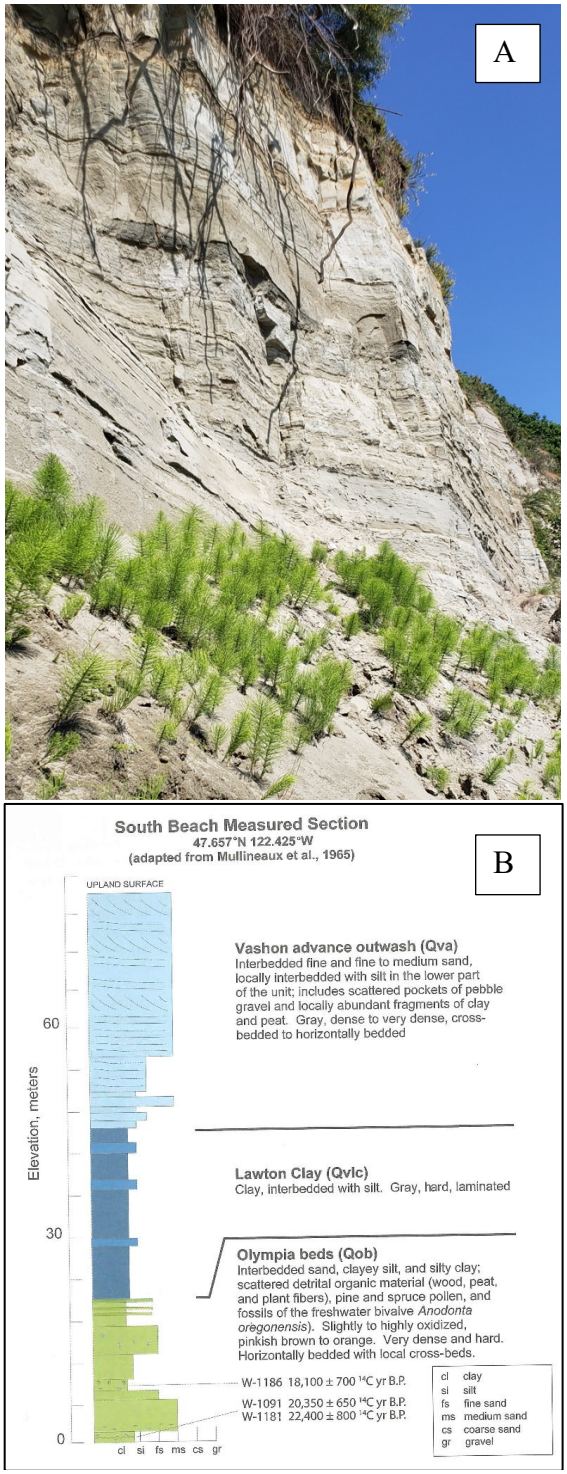

Figure 4. A (upper) - South facing bluff at Discovery Park composed of Lawton Clay. The sampling location was exposed by a recent landslide as evidenced by the lack of vegetation, with the exception of horsetails on the colluvial apron. **B** (lower) – Measured section of Vashon glacial sediments at Discovery Park. (Adapted from Troost and Booth, 2008)

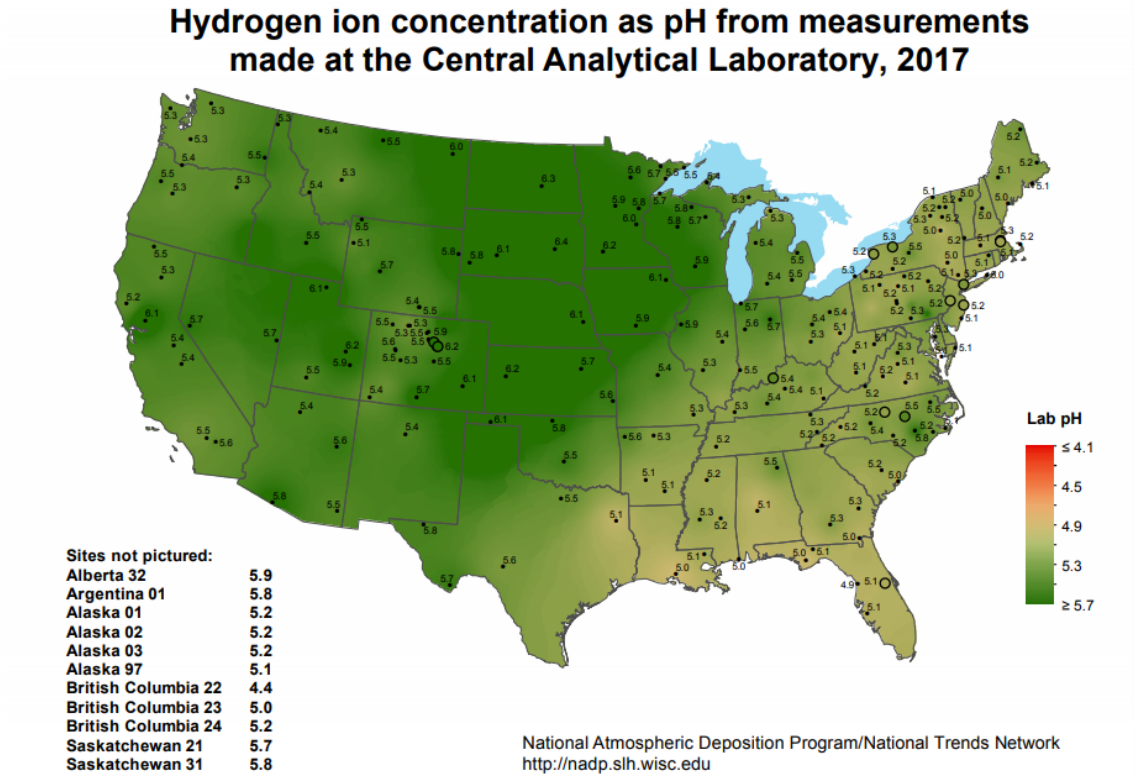

Figure 5. Atmospheric hydrogen ion concentration for the continental US. Figure from National Atmospheric Deposition Program.

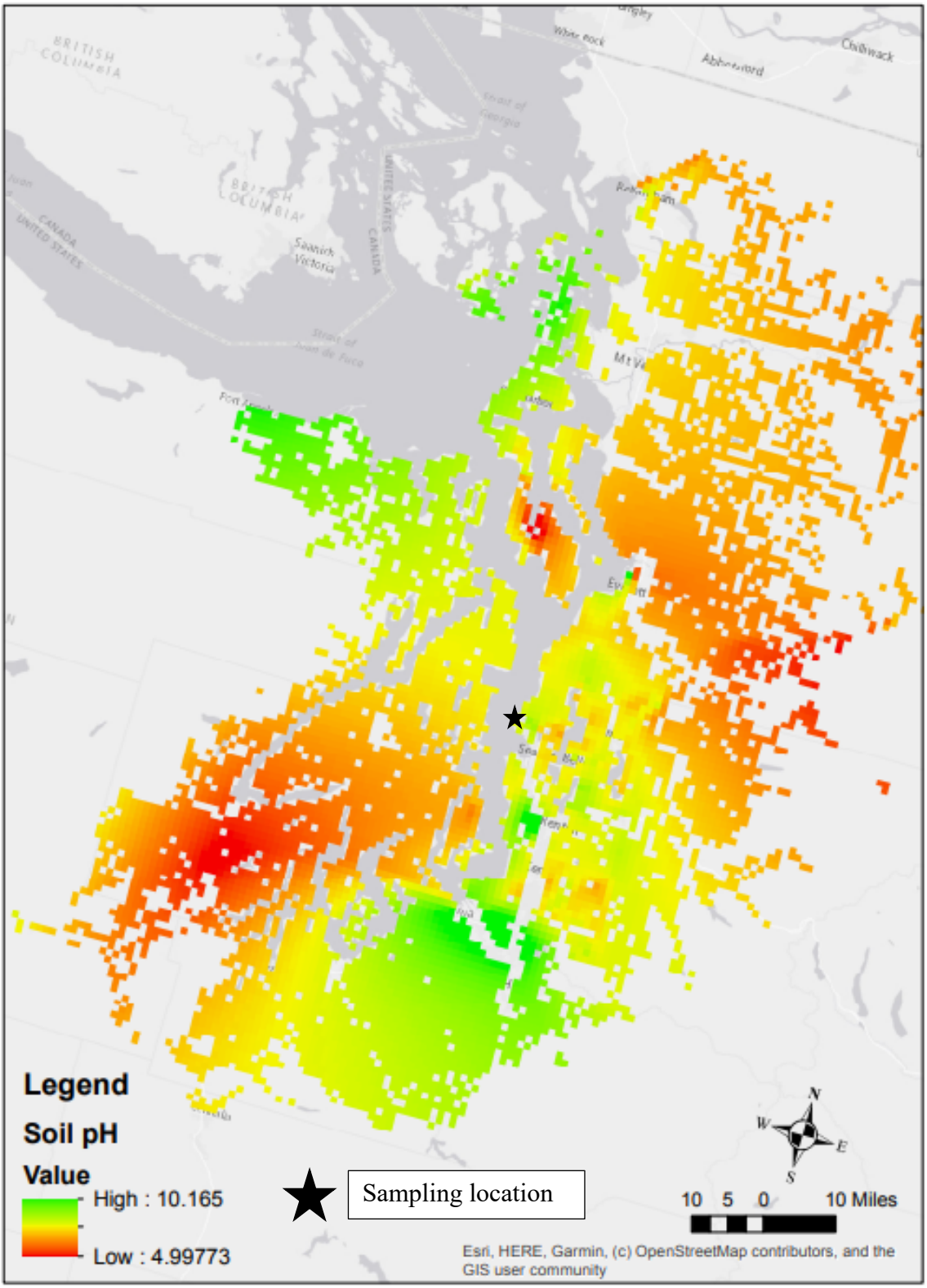

Figure 6. Interpolated soil pH values generated from Washington Department of Ecology wet soil pH measurements. Predicted pH at sampling site is shown as near neutral (7).

Figure 7. Location map of Discovery Park, Seattle, Washington the type section for the Lawton Clay. The inset map shows the sampling locations on the South Beach Bluff of Discovery Park.

Figure 8. Large block of Lawton Clay extracted from south-southwest exposed bluff at Discovery Park.

Figure 9. Partially crushed, homogenized sample of Lawton Clay spread out on a tarp in a horse trailer to dry.

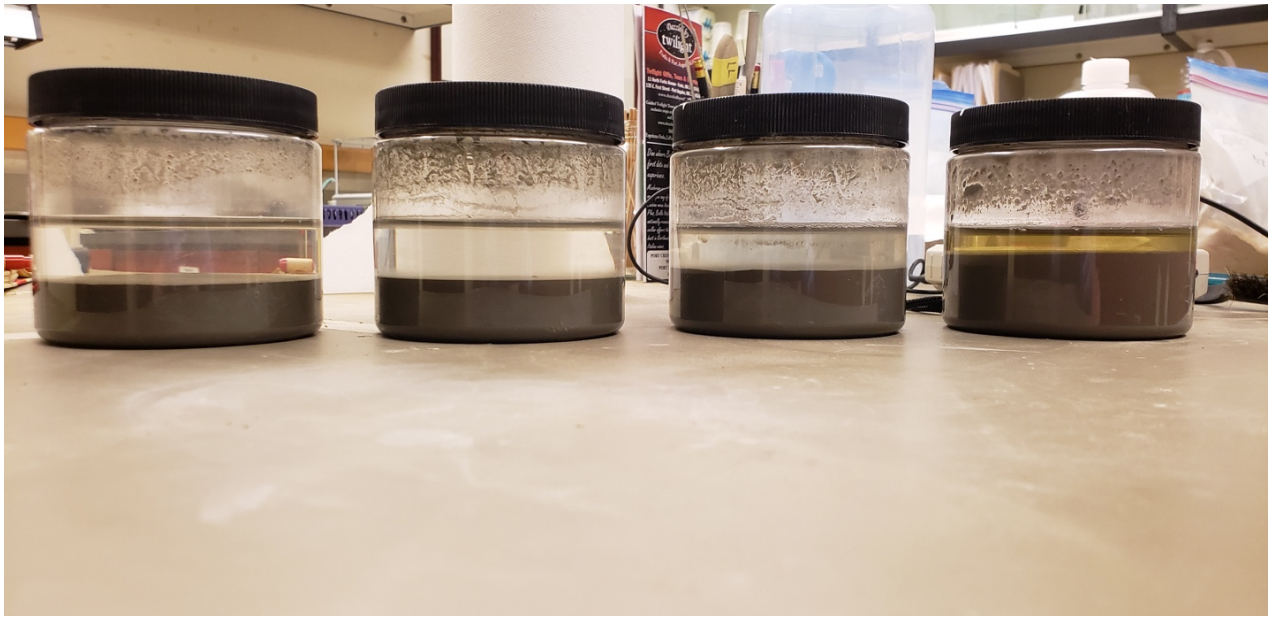

Figure 10. Soil samples rehydrated with sulfuric acid solutions to test buffer capacity. The pH of the samples are 2.52, 1.91, 0.92, and 0.0 from left to right. Each sample has 200 mL of solution and 120 g of soil. Notice the decreased consolidation at lower pH values.

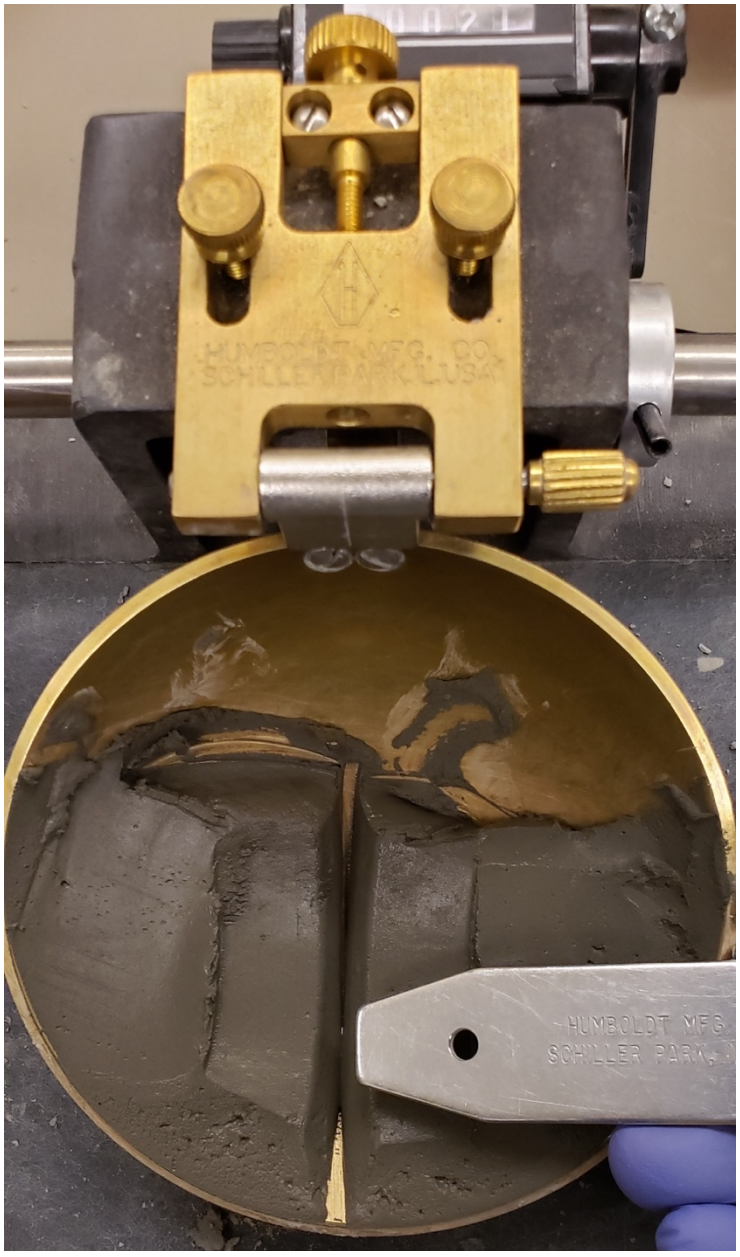

Figure 11. Soil pat groove cut by the standard grooving tool closed a distance of 12.7 mm (0.5 in). This test took 21 blows to close the groove as shown by the counter at the top of the image.

Figure 12. Rehydrated soil pat spread out on frosted glass to lower moisture content.

Figure 13. Thread of soil breaking apart at a diameter of 3.2 mm (~1/8 in.). This thread is at the plastic limit.

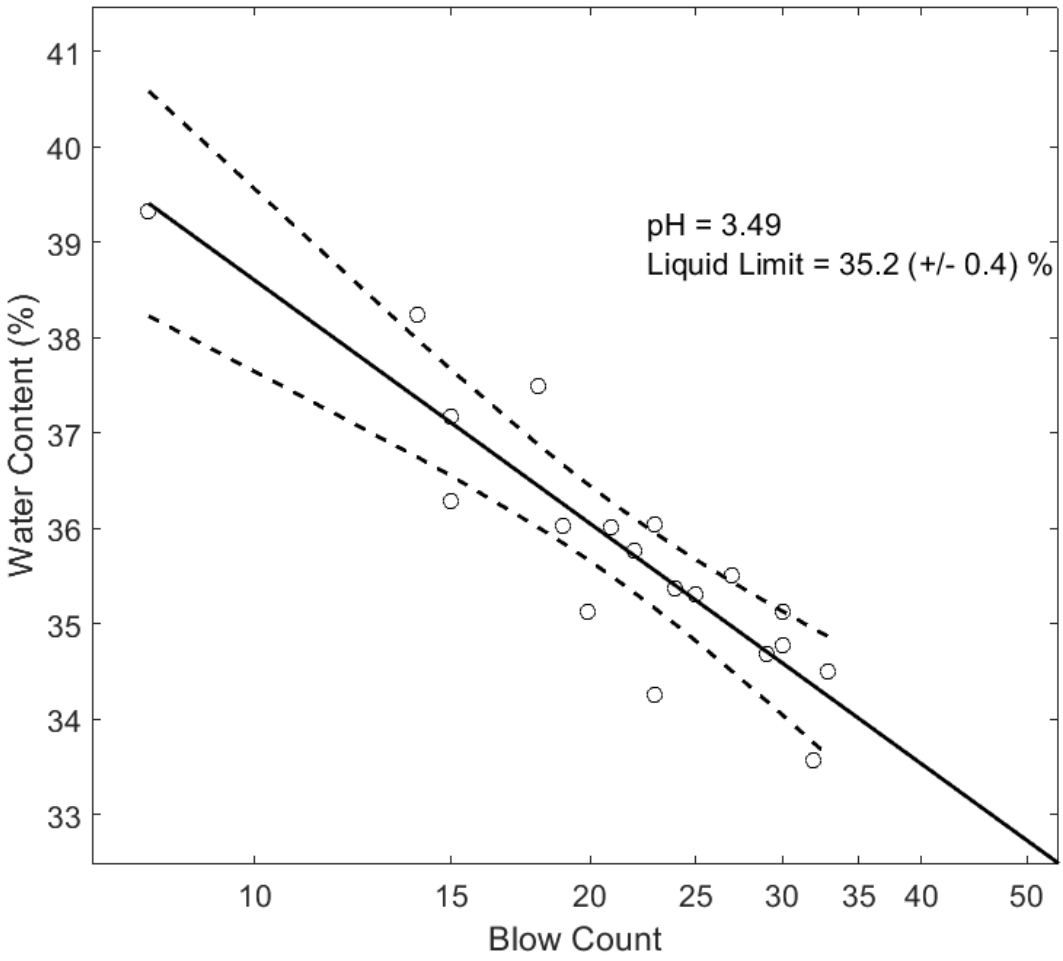

Figure 14. Water content as a function of blow count for the Atterberg 3-point liquid limit test. Results from six separate runs for a pH of 3.49 are plotted as open circles. The solid line is a linear fit of all data. The dashed lines give 95% confidence intervals for the fit. The blow count axis is logarithmic.

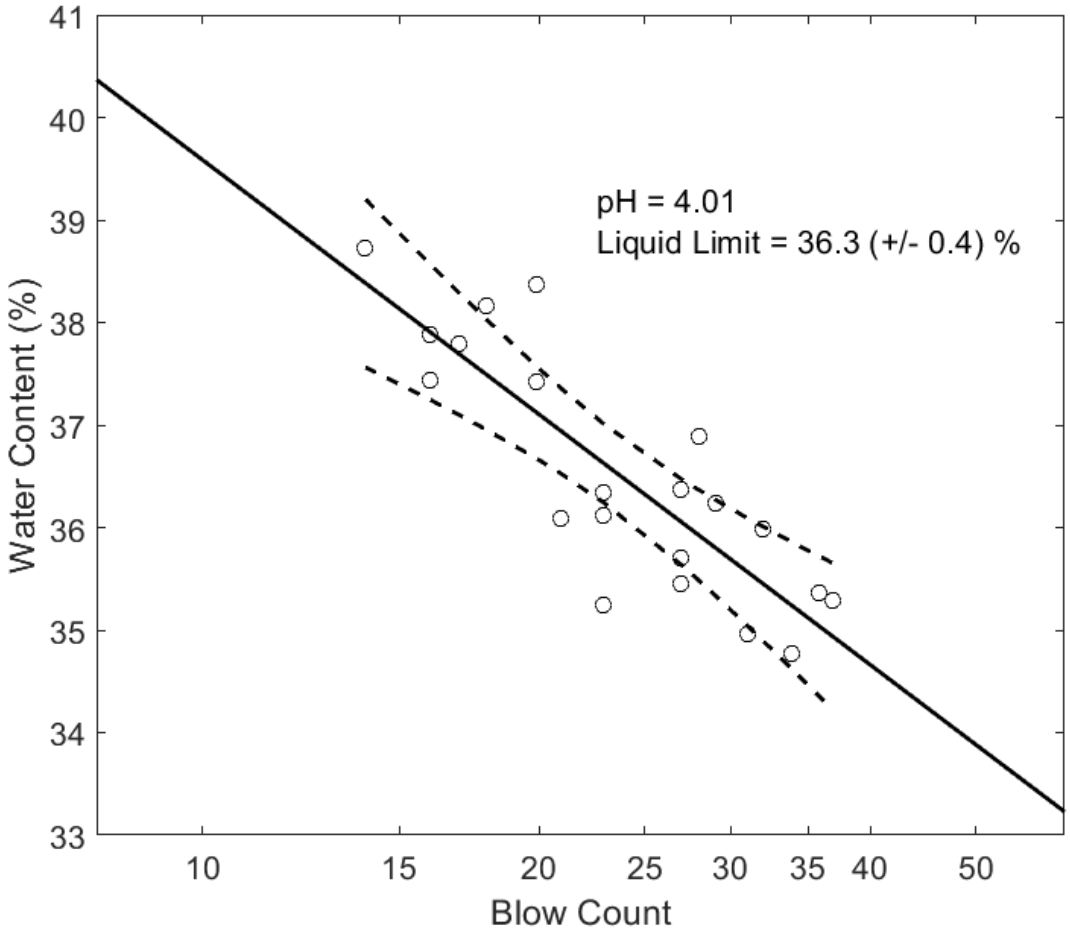

Figure 15. Water content as a function of blow count for the Atterberg 3-point liquid limit test. Results from seven separate runs for a pH of 4.01 are plotted as open circles. The solid line is a linear fit of all data. The dashed lines give 95% confidence intervals for the fit. The blow count axis is logarithmic.

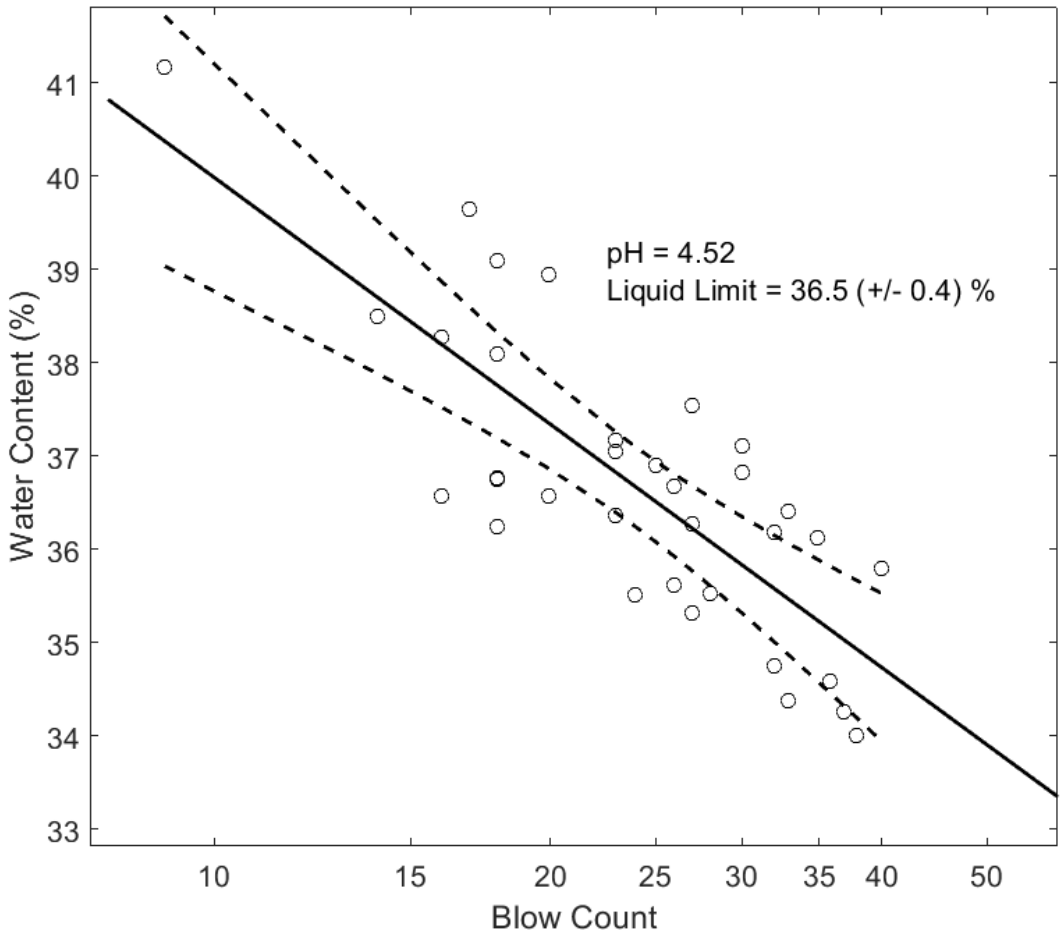

Figure 16. Water content as a function of blow count for the Atterberg 3-point liquid limit test. Results from eleven separate runs for a pH of 4.52 are plotted as open circles. The solid line is a linear fit of all data. The dashed lines give 95% confidence intervals for the fit. The blow count axis is logarithmic.

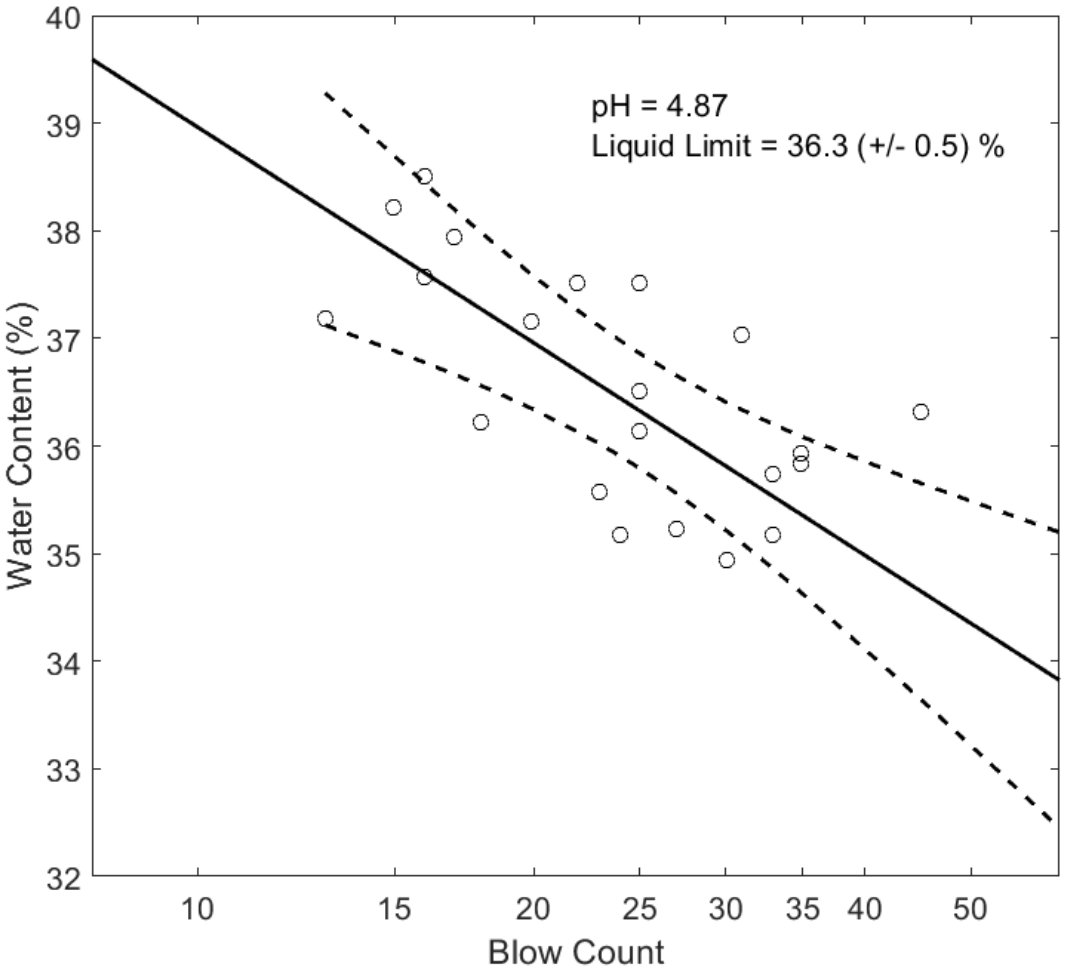

Figure 17. Water content as a function of blow count for the Atterberg 3-point liquid limit test. Results from seven separate runs for a pH of 4.87 are plotted as open circles. The solid line is a linear fit of all data. The dashed lines give 95% confidence intervals for the fit. The blow count axis is logarithmic.

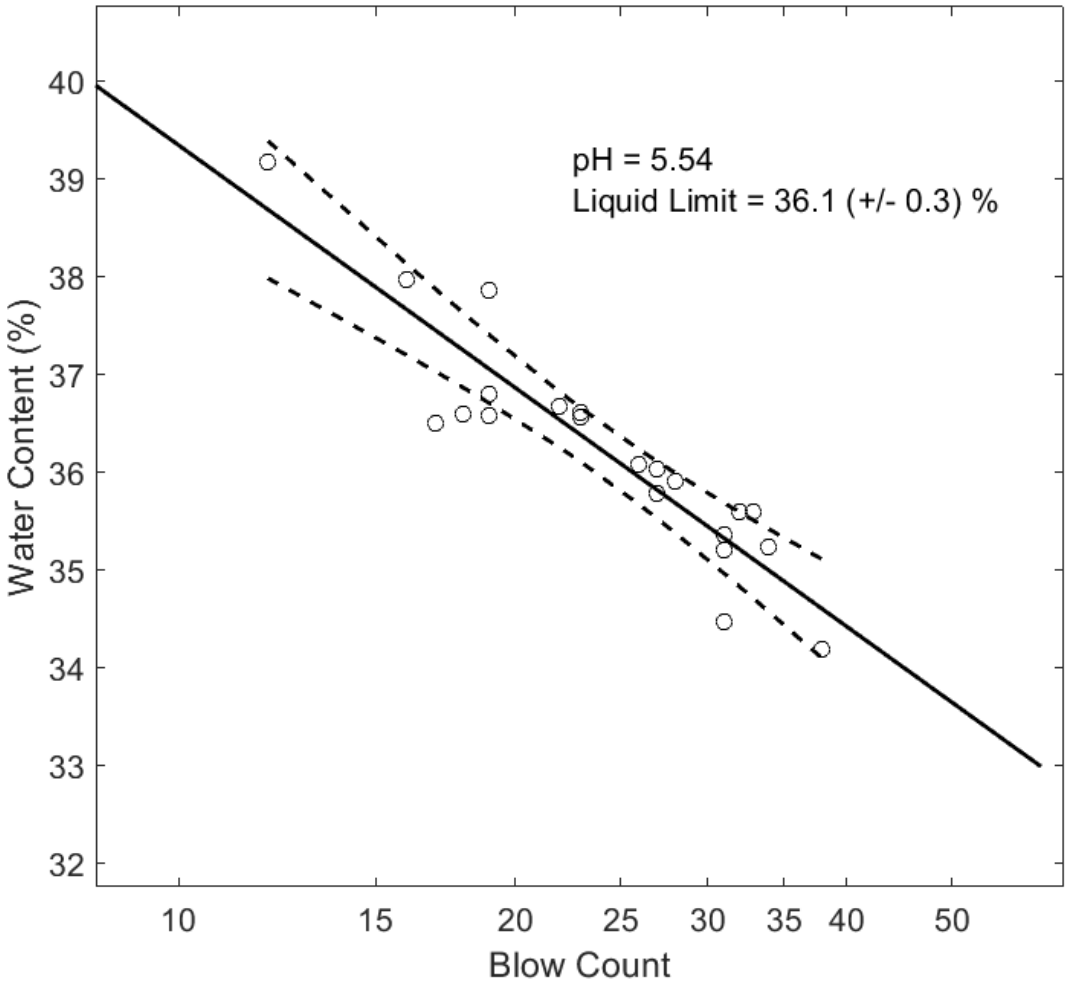

Figure 18. Water content as a function of blow count for the Atterberg 3-point liquid limit test. Results from seven separate runs for a pH of 5.54 are plotted as open circles. The solid line is a linear fit of all data. The dashed lines give 95% confidence intervals for the fit. The blow count axis is logarithmic.

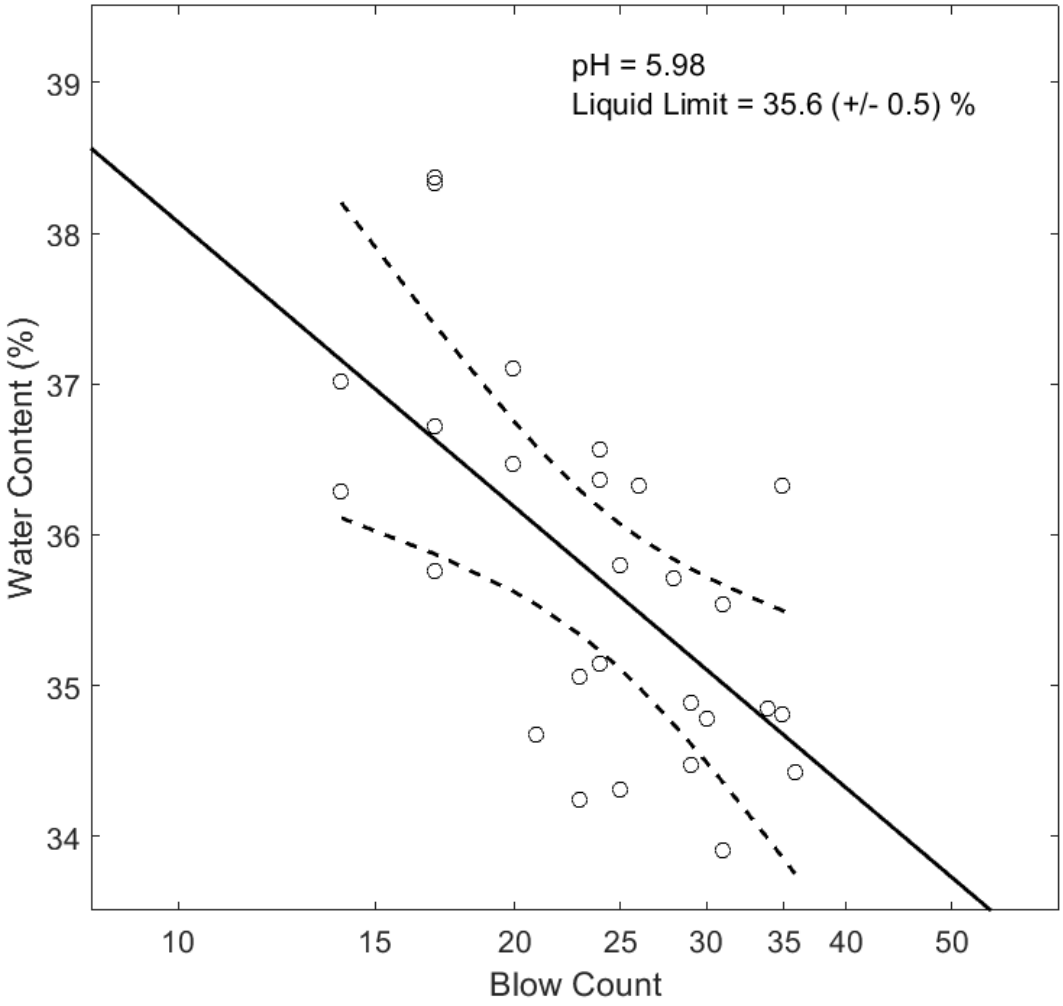

Figure 19. Water content as a function of blow count for the Atterberg 3-point liquid limit test. Results from nine separate runs for a pH of 5.98 are plotted as open circles. The solid line is a linear fit of all data. The dashed lines give 95% confidence intervals for the fit. The blow count axis is logarithmic.

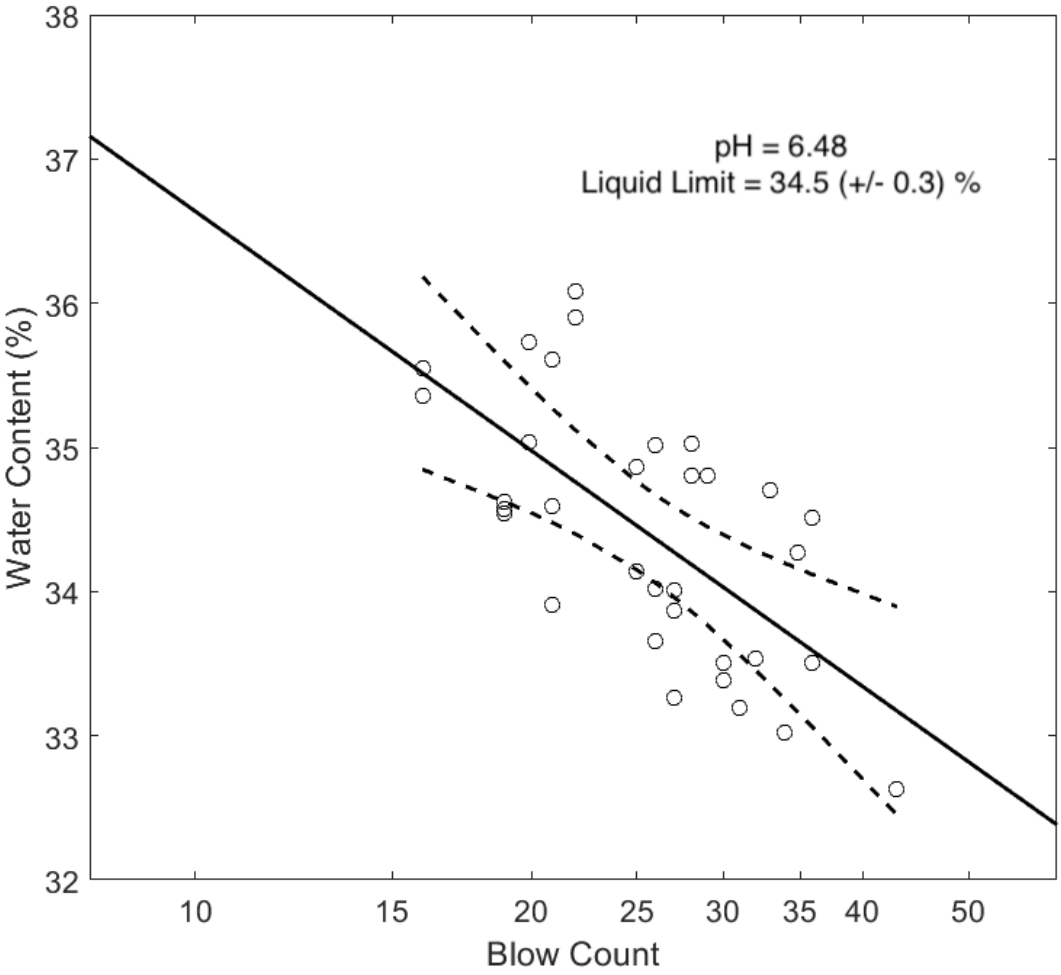

Figure 20. Water content as a function of blow count for the Atterberg 3-point liquid limit test. Results from eleven separate runs for a pH of 6.48 are plotted as open circles. The solid line is a linear fit of all data. The dashed lines give 95% confidence intervals for the fit. The blow count axis is logarithmic.

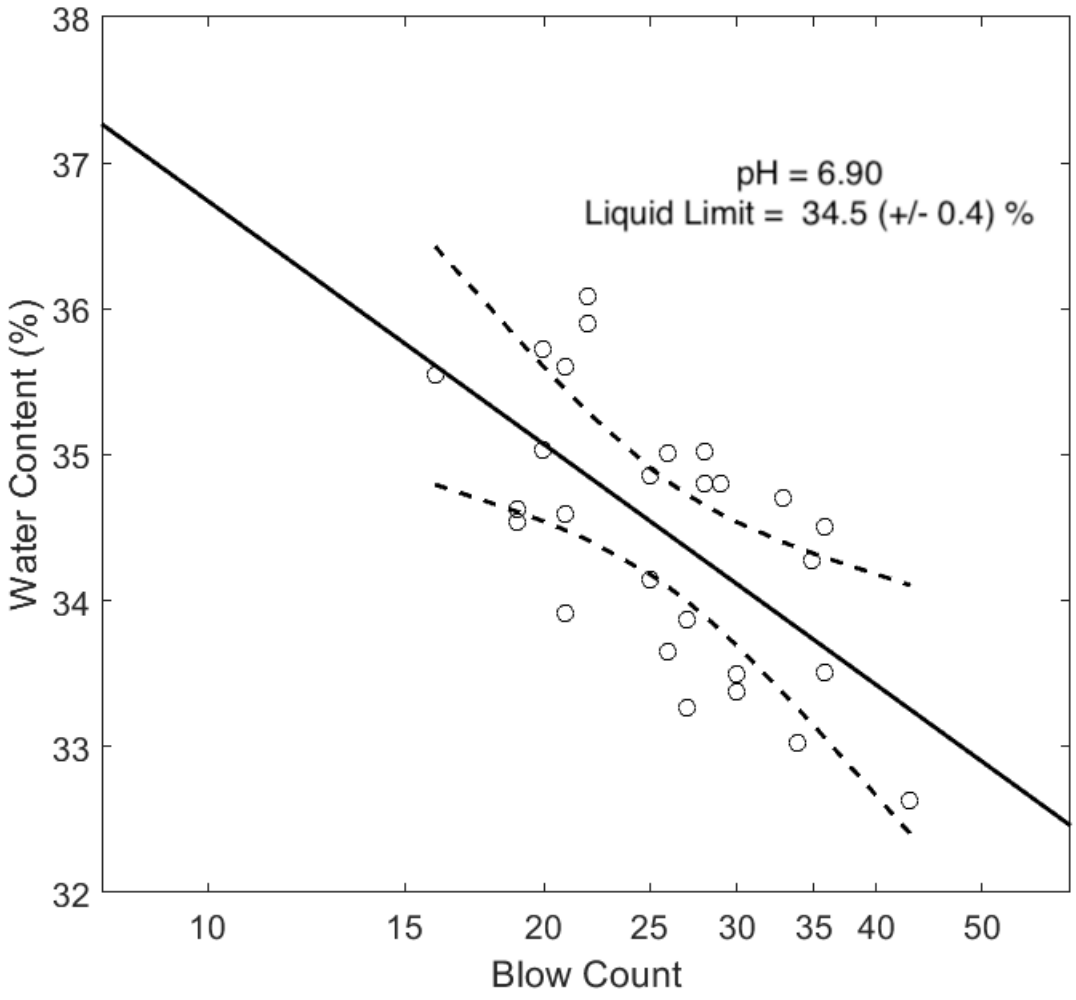

Figure 21. Water content as a function of blow count for the Atterberg 3-point liquid limit test. Results from nine separate runs for a pH of 6.90 are plotted as open circles. The solid line is a linear fit of all data. The dashed lines give 95% confidence intervals for the fit. The blow count axis is logarithmic.

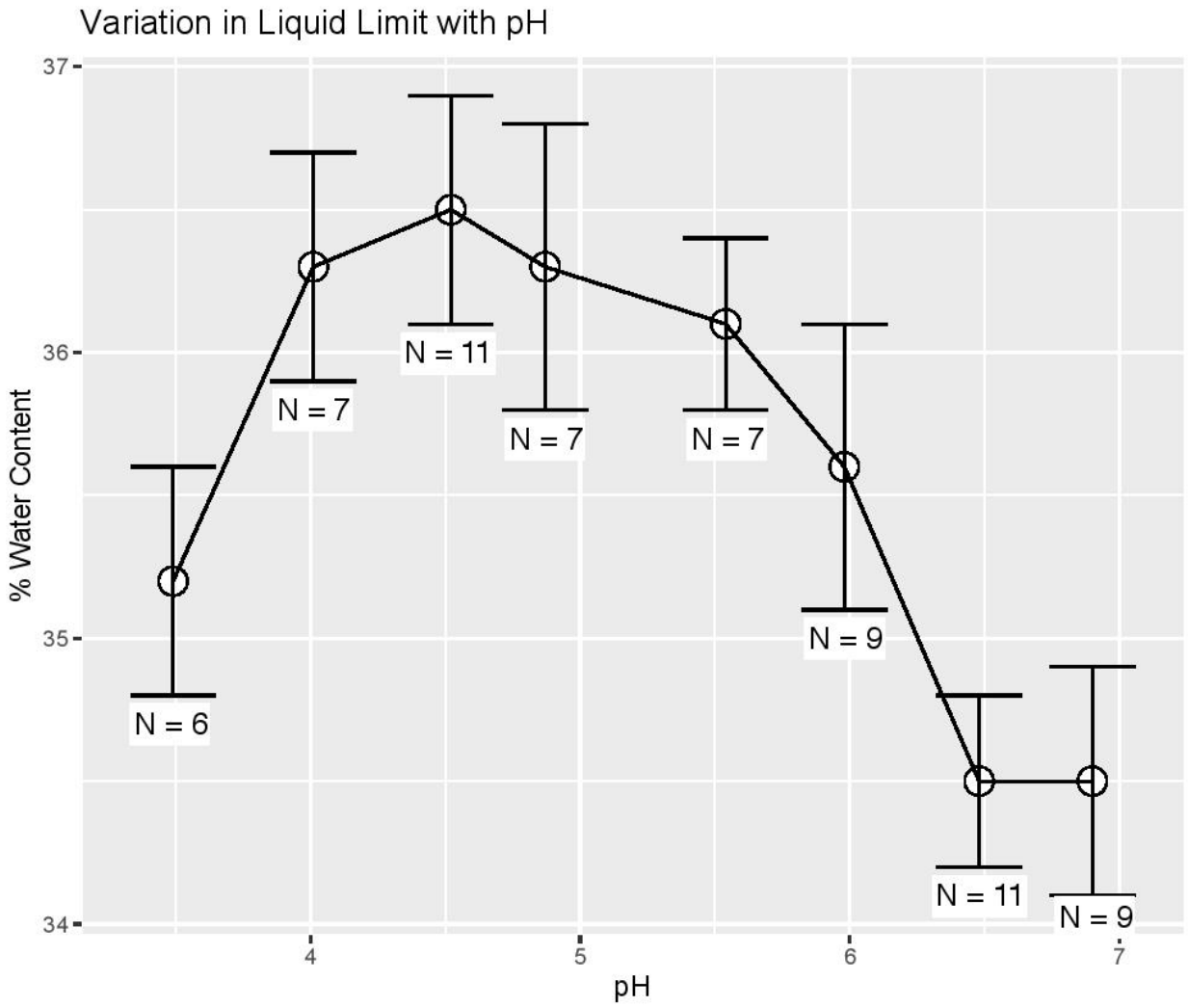

Figure 22. Plot of liquid limit vs. pH. Error bars show 95% confidence interval.

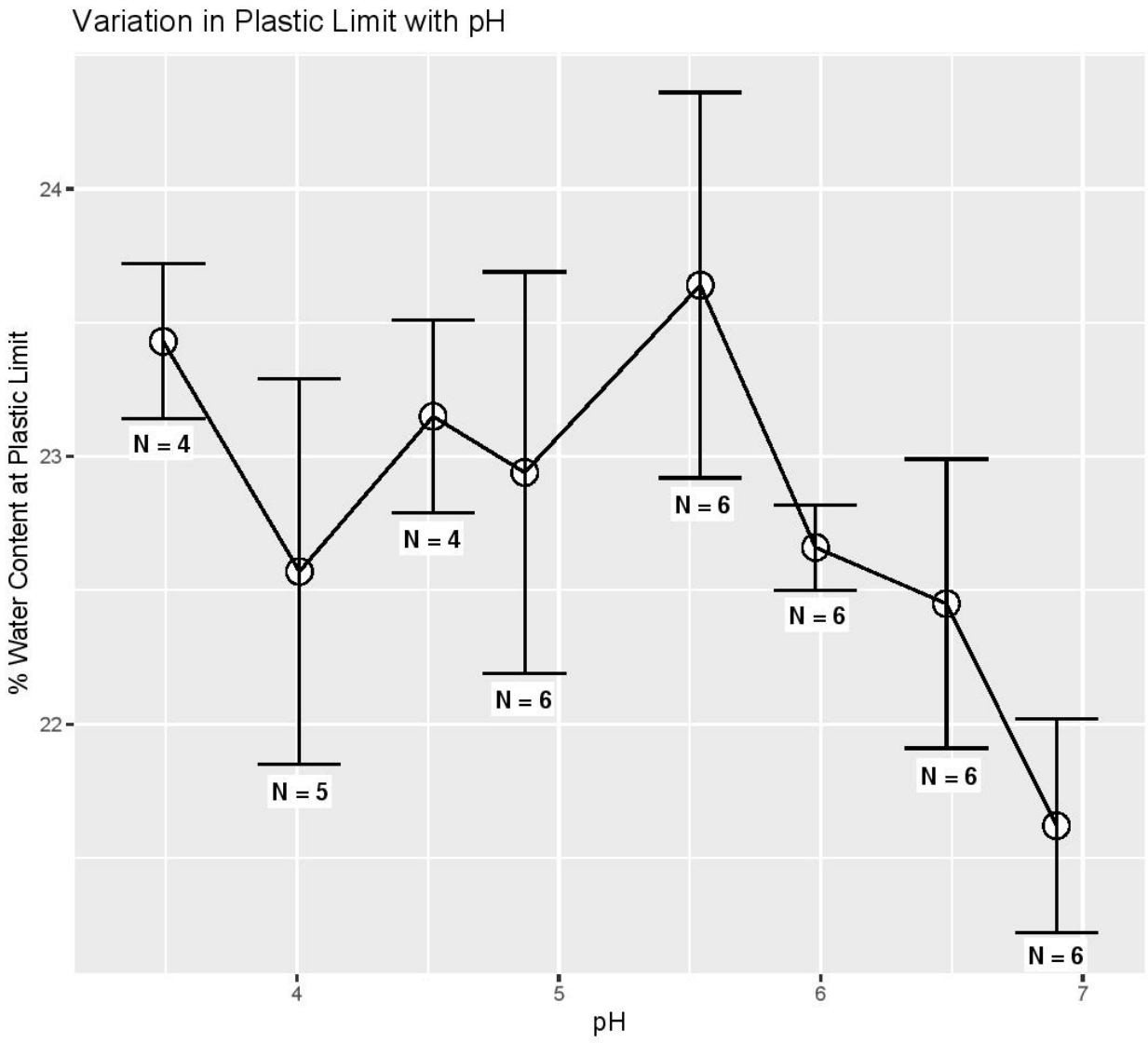

Figure 23. Plot of plastic limit vs. pH. Error bars show one standard deviation from the average.

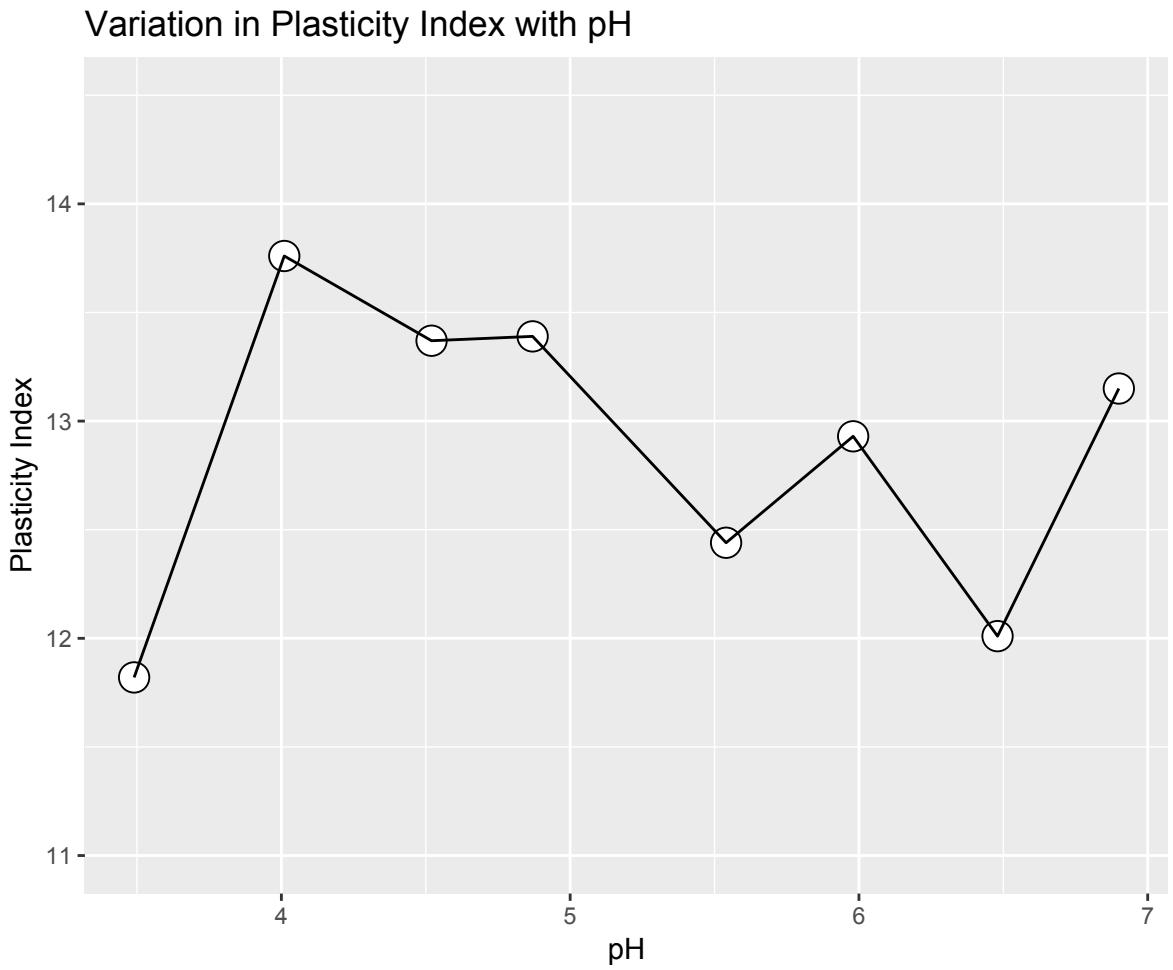

Figure 24. Plot of plasticity index vs. pH. The plasticity index is equal to the predicted liquid limit minus the average plastic limit.

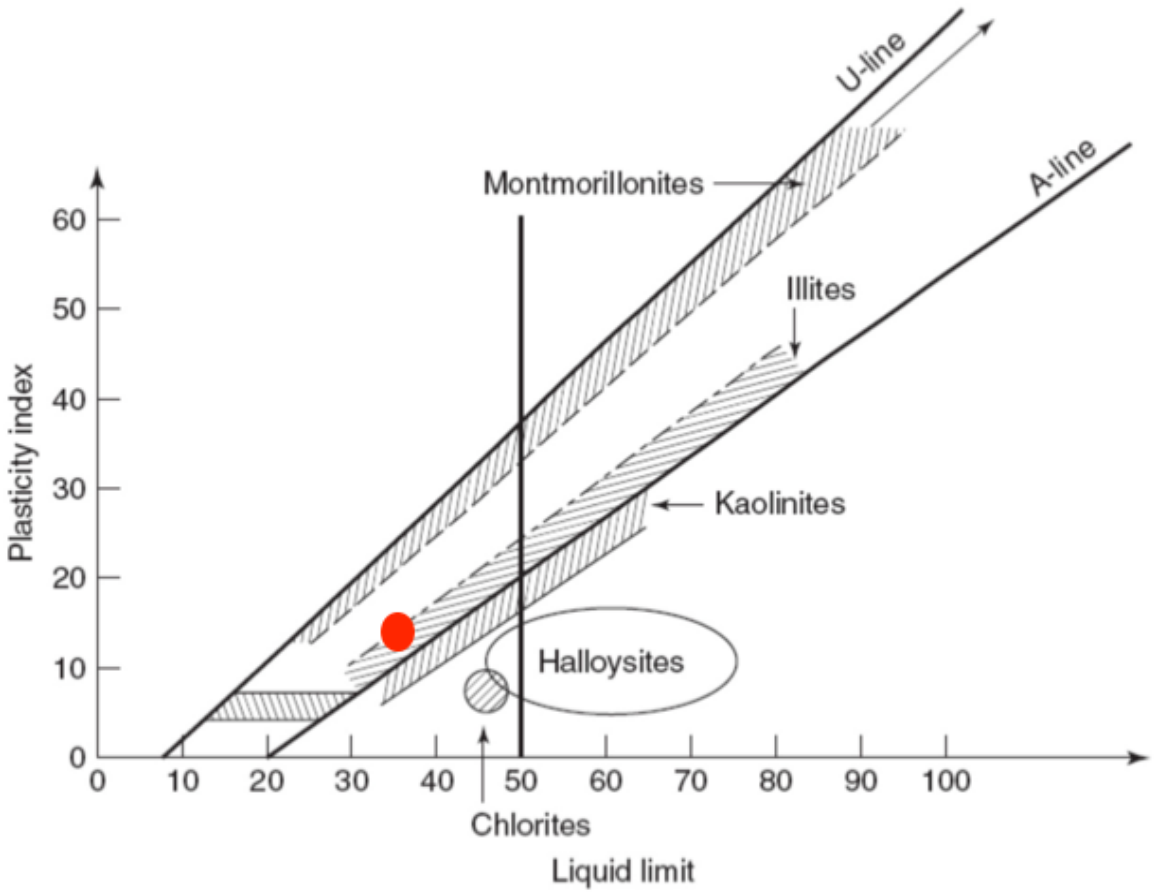

Figure 25. All of the samples (pH 3.5 – 7) plot within the illite clay mineral group. Mullineaux (1967) and Gault (2015) found the clay minerals present in the Lawton Clay to be chlorite, illite and smectite in order of decreasing abundance. Base image from Mitchell, 1993.

Tables

Table 1. Cation exchange capacity (CEC) of dry homogenized samples measured by the Analytical Service Center, School of Environmental and Forest Sciences, University of Washington. Meq/100 g is milliequivalent per 100 g.

Sample Number	CEC (meq/100 g)
1	10.99
2	11.56
3	13.24
4	11.48
5	14.25
6	10.91

Table 2. A) Anion concentrations of Seattle rainwater measured by Root et al. B) Molarity of H+ ion of the protonated anion. C) Proportions (in % molarity) of H+ ions. These proportions are conserved during the dilution process.

	Chloride (Cl^-)	Nitrate (NO_3^-)	Sulfate (SO_4^{2-})
A) Concentration from Root et al. 2004	0.3449 (mg/L)	2.159 (mg/L)	4.1267 (mg/L)
B) Molarity of H+	$9.87X10^{-6}$ (mol/L)	$3.48X10^{-5}$ (mol/L)	$8.60X10^{-5}$ (mol/L)
C) Molar Proportions	7.6%	26.6%	65.8%

Table 3. pH of the rehydrated samples prior to and after Atterberg Limit testing. These data show that the progressive drying associated with the tests had a minor effect on the sample pH.

pH of Samples Prior to Atterberg Limit Tests	pH of Samples (Untested Material) after Atterberg Limit Tests
3.49	3.65
4.01	4.13
4.52	4.51
4.87	4.87
5.54	5.52
5.98	6.10
6.48	6.41
6.90	6.82

Table 4. Predicted liquid limit values and associated prediction error. Liquid limits were predicted from a regression line through multiple runs of the 3-point liquid limit test results.

pH	Predicted Liquid Limit	Error from Confidence Interval (+/-)
3.49	35.2	0.4
4.01	36.3	0.4
4.52	36.5	0.4
4.87	36.3	0.5
5.54	36.1	0.3
5.98	35.6	0.5
6.48	34.5	0.3
6.90	34.5	0.4

Table 5. Plastic limit values and σ and 2σ of error from average.

pH	Average Plastic Limit	σ (+/-)	2σ (+/-)
3.49	21.6	0.4	0.8
4.01	22.5	0.5	1.1
4.52	22.7	0.2	0.3
4.87	23.6	0.7	1.4
5.54	22.9	0.8	1.5
5.98	23.2	0.4	0.7
6.48	22.6	0.7	1.4
6.90	23.4	0.3	0.6

Table 6. Plasticity index values based on average liquid and plastic limits.

pH	Plasticity Index
3.49	11.8
4.01	13.8
4.52	13.4
4.87	13.4
5.54	12.4
5.98	12.9
6.48	12.0
6.90	13.2

Appendix

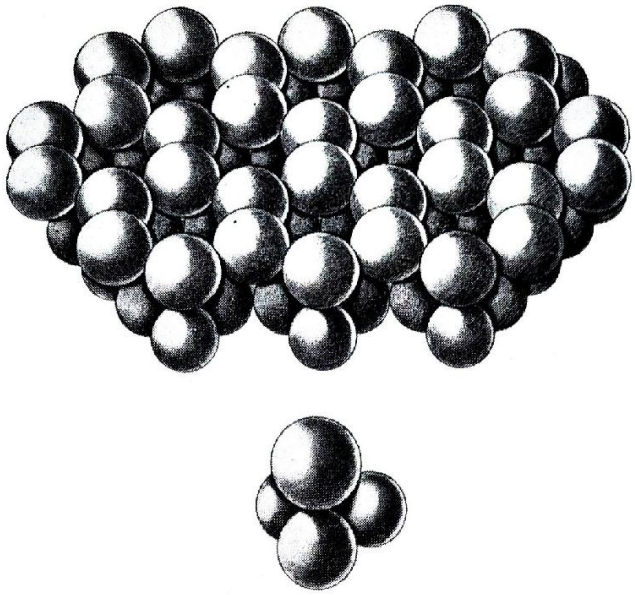

Fig. 17*a*. Model of silicon-oxygen tetrahedron and of the tetrahedral sheet.

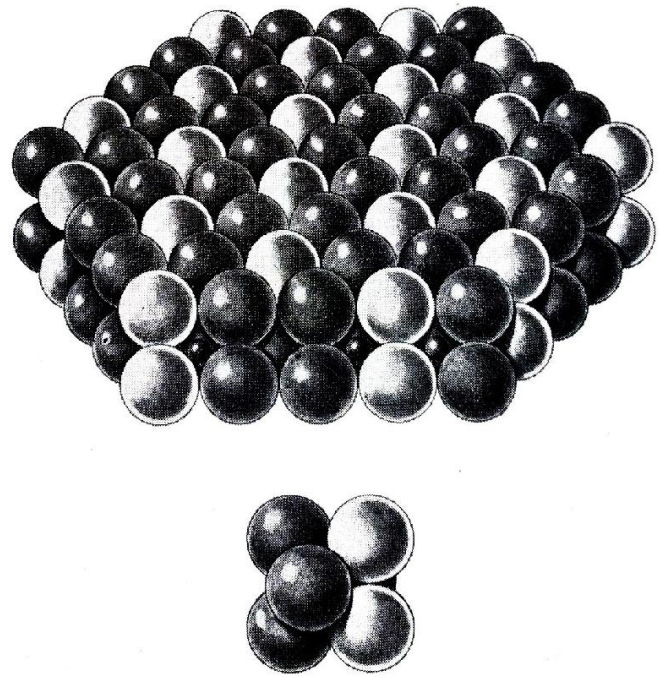

Fig. 17*b*. Model of aluminum-oxygen octahedron and of the octahedral sheet. (In this sketch, hydroxyl groups have been given a lighter shading.)

Figure A-1. Models of clay mineral crystals. From Van Olphen, 1963

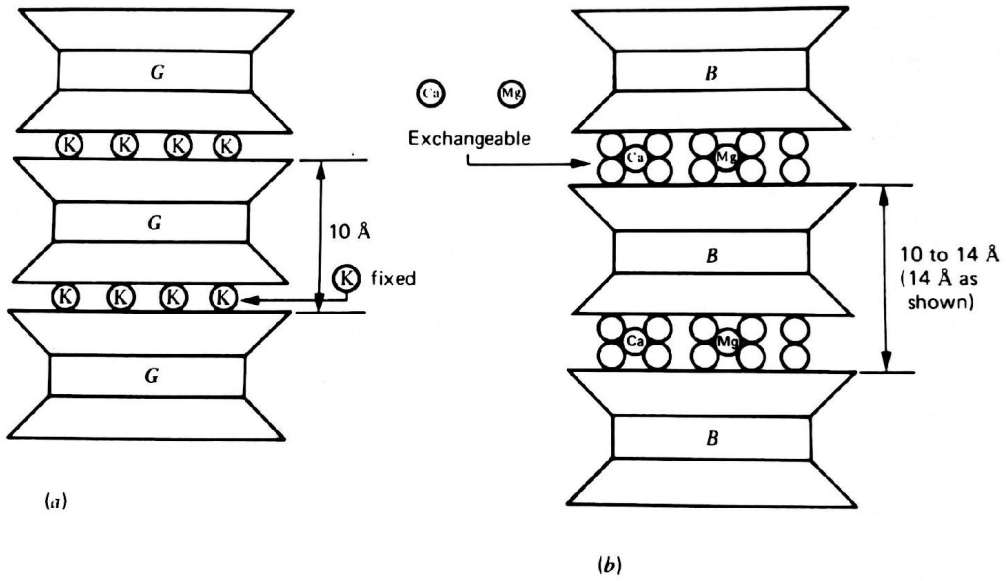

Figure 3.19 Schematic diagram of the structures of muscovite, illite, and vermiculite. (*a*) Muscovite and illite. (*b*) Vermiculite.

Figure A-2. Cations K = Potassium, Ca = Calcium, Mg = Magnesium. From Mitchell, 1993.

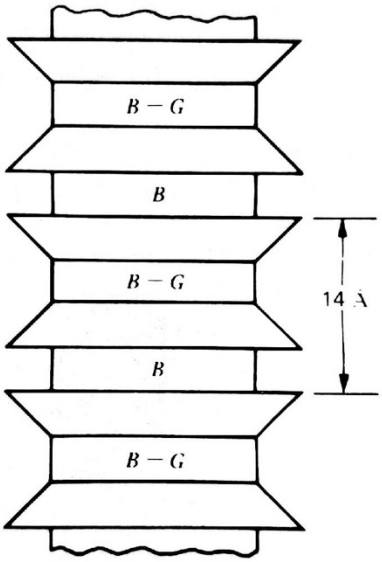

Figure 3.23 Schematic design of the structure of chlorite.

Figure A-3. B = Brucite like octahedral sheet, G = Gibbsite. From Mitchell, 1993.

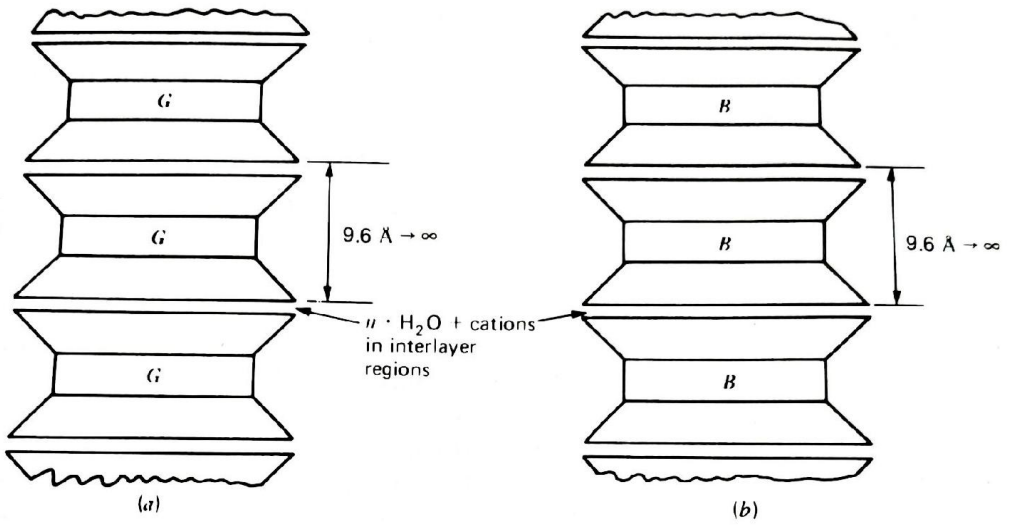

Figure 3.15 Schematic diagrams of the structures of the smectite minerals (*a*) Montmorillonites. (*b*) Saponites.

Figure A-4. Hydration of interlayer regions results in swelling. From Mitchell, 1993.

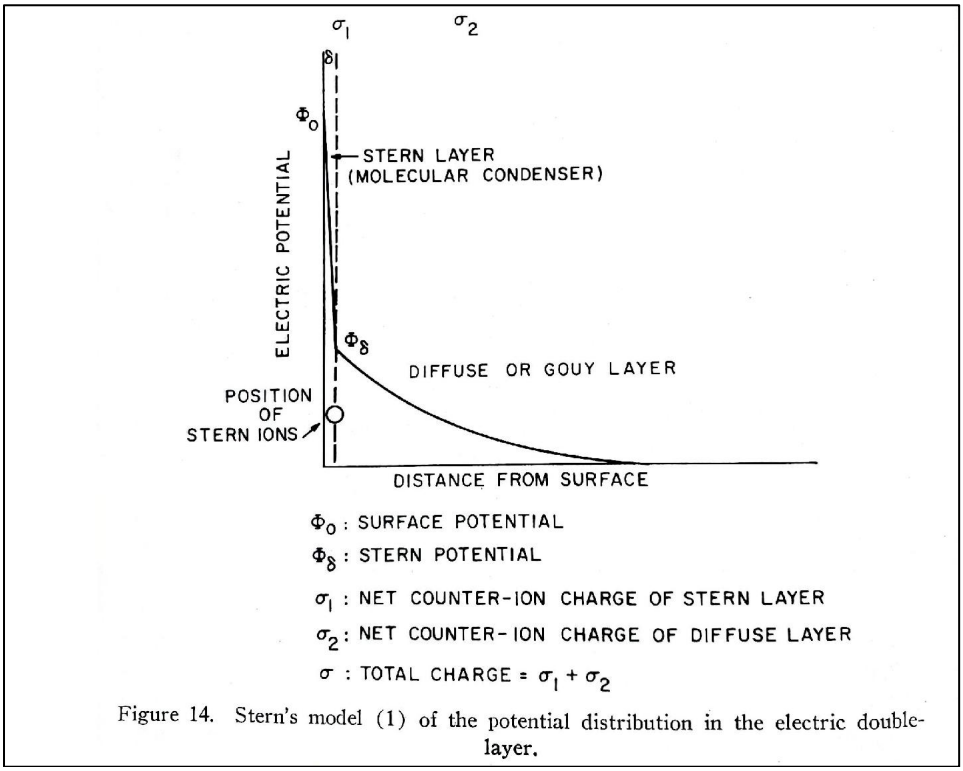

Figure 14. Stern's model (1) of the potential distribution in the electric double-layer.

Figure A-5. Stern model for double diffuse layer. From Van Olphen, 1963

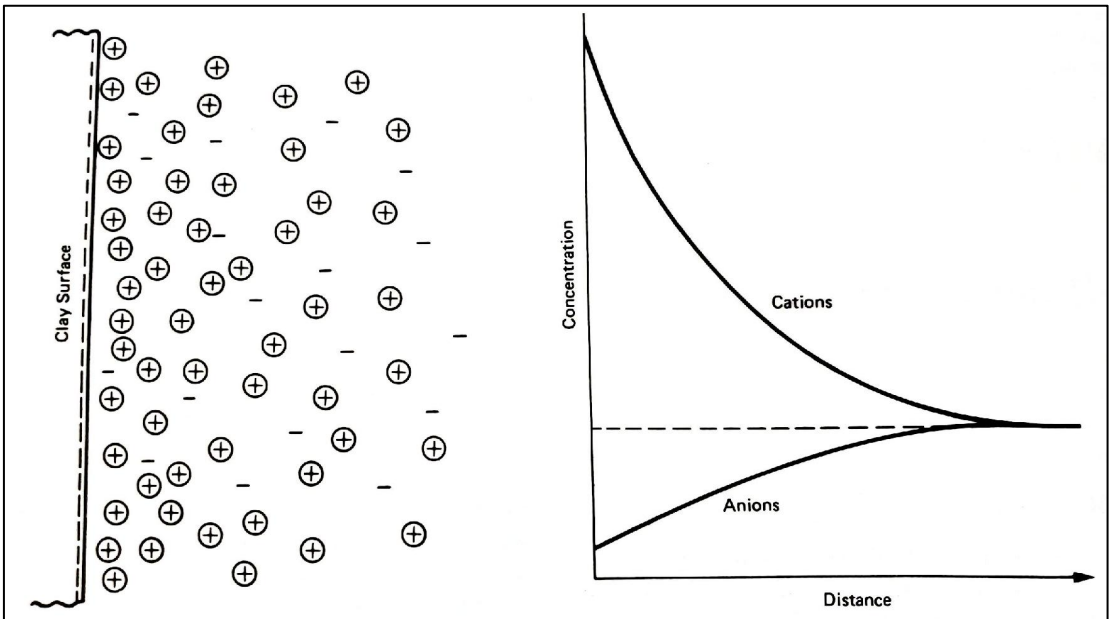

Figure 7.1 Distributions of ions adjacent to a clay surface according to the concept of the diffuse double layer.

Figure A-6. Conceptual model of ion concentration adjacent to the clay surface. From Mitchell, 1993

Equation 1

Electric potential at surface: $\phi = \frac{kT}{ve} \ln\left(\frac{c}{c_0}\right)$

- k = Boltzmann constant
- T = Absolute temperature
- e = Electronic charge
- ν = Ion valence
- c = Ion concentration in solution
- c_0 = Ion concentration at zero point of charge when $\phi = 0$

Equation 2

Thickness* of the double diffuse layer ($\frac{1}{K}$): $\frac{1}{K} = \sqrt{\left(\frac{\epsilon_0 DkT}{2n_0 e^2 \nu^2}\right)}$

- ϵ_0 = permittivity of a vacuum
- D = dielectric constant of the medium
- k = Boltzman constant
- T = Temperature (K°)
- n_0 = electrolyte concentration
- ν^2 = cation valence

*Thickness refers to the center of gravity of diffuse charge

Equation 3

Mohr Coulomb Strength Envelope: $\tau_s = C + \sigma \tan \phi$

- τ_s = Shear strength
- C = Cohesion
- σ = Normal stress
- ϕ = Friction angle